Molecular Therapy
Original Article

CTRP1 regulates skeletal muscle differentiation through quality control of mitochondrial dynamics and function

Sora Han,[1] Youjeong Jang,[2] Hyun Jeong Joo,[2] Hye In Ka,[1,7] Se Hwan Mun,[1] Hai-Anh Nguyen,[1] Doyeon Park,[2] Yoohyun Jung,[2] Doyeong Ko,[1] Bo Ram Sohn,[1] Seong Keun Sonn,[3] Goo Taeg Oh,[3] Young-Chul Choi,[4] So-Young Park,[5] Sung-Eun Kim,[6] and Young Yang[1,2]

[1]Research Institute of Women's Health, Sookmyung Women's University, Seoul, Korea; [2]Department of Biological Sciences, Sookmyung Women's University, Seoul, Korea; [3]Department of Life Sciences, Ewha Womans University, Seoul, Korea; [4]Department of Neurology, Gangnam Severance, College of Medicine, Yonsei University, Seoul, Korea; [5]Department of Physiology, College of Medicine, Yeungnam University, Daegu, Korea; [6]Department of Food and Nutrition, Sookmyung Women's University, Seoul, Korea

Mitochondrial dysfunction is a hallmark of myopathies and impaired skeletal muscle differentiation. Here, we demonstrate that C1q/TNF-related protein 1 (CTRP1) is essential for maintaining mitochondrial dynamics and supporting myogenic differentiation. Loss of CTRP1 in myoblasts and in skeletal muscle-specific-knockout (CTRP1 KO$^{\Delta ACTA}$) mice led to impaired myotube formation, reduced muscle fiber cross-sectional area, and decreased muscle strength. CTRP1 deficiency also shifted the muscle fiber composition from oxidative type IIA to glycolytic type IIB fibers, indicating a compromised mitochondrial capacity. At the cellular level, CTRP1 loss resulted in elongated and disorganized mitochondria with diminished cristae density, membrane potential, and oxidative respiration. These mitochondrial abnormalities are associated with defective recruitment of dynamin-related protein 1 (DRP1), a central mediator of mitochondrial fission. Restoring CTRP1 expression or performing mitochondrial transplantation in CTRP1-KO myoblasts rescued mitochondrial function and re-established differentiation capacity. Furthermore, CTRP1 expression progressively decreased in accordance with disease severity in skeletal muscle biopsies from patients with polymyositis, dermatomyositis, and Duchenne muscular dystrophy, supporting its potential relevance to human myopathies. Together, these findings identify CTRP1 as a novel regulator of mitochondrial quality and myogenic differentiation, highlighting its potential as a therapeutic target for mitochondrial myopathies.

INTRODUCTION

Skeletal muscle diseases, or myopathies, comprise a heterogeneous group of disorders characterized by muscle weakness, degeneration, and metabolic dysfunction. These include genetic forms such as muscular dystrophies and channelopathies, as well as acquired conditions such as inflammatory, endocrine, and toxin-induced myopathies.[1] Among these, mitochondrial and metabolic myopathies are complex due to their diverse clinical presentations and impaired oxidative metabolism. This impairment in oxidative metabolism compromises mitochondrial ATP production, contributing to the energy deficiency that underlies the hallmark features of myopathies, such as fatigue, muscle atrophy, and exercise intolerance.[2]

Mitochondrial dysfunction is now recognized as a prevalent feature of genetic and acquired myopathies. This dysfunction often involves abnormalities in mitochondrial dynamics, including fusion, fission, biogenesis, and mitophagy.[3] These processes are essential for maintaining cellular energy homeostasis, limiting oxidative stress, and supporting muscle regeneration, particularly by enabling energy-intensive steps such as myogenic differentiation.[4] Among the aspects of mitochondrial dynamics, mitochondrial fission plays a critical role in mitochondrial quality control and facilitates metabolic adaptation during myogenic differentiation.[4] This mitochondrial fission process is primarily mediated by the cytosolic GTPase dynamin-related protein 1 (DRP1), which is recruited to the mitochondrial outer membrane to mediate division.[5] Proper DRP1 localization preserves mitochondrial morphology and function, whereas fission failure leads to the accumulation of elongated dysfunctional mitochondria and contributes to muscle degeneration.[6]

A set of four mitochondrial outer membrane proteins, including mitochondrial fission protein 1 (Fis1), mitochondrial fission factor (Mff), and mitochondrial dynamics proteins of 49 and 51 kDa (MiD49/51), have been identified as potential adaptors that facilitate the recruitment of DRP1 to the mitochondrial surface for fission.[7,8]

Received 24 May 2025; accepted 30 December 2025;
https://doi.org/10.1016/j.ymthe.2025.12.063.

[7]Present address: Department of Physiology, Ajou University School of Medicine, Suwon, Korea

Correspondence: Young Yang, Research Institute of Women's Health, Sookmyung Women's University, Seoul, Korea.
E-mail: yyang@sookmyung.ac.kr

Published by Elsevier Inc. on behalf of The American Society of Gene and Cell Therapy.
This is an open access article under the CC BY-NC-ND license (http://creativecommons.org/licenses/by-nc-nd/4.0/).

However, despite increasing interest, the molecular players that mediate the physical and functional coupling between the endoplasmic reticulum (ER) and mitochondria remain poorly understood. Recent evidence has identified C1q/TNF-related protein 1 (CTRP1), an ER-associated protein, as a novel factor that induces DRP1 recruitment to ER-mitochondrial contact sites in Purkinje and retinal ganglion cells.[9] Loss of CTRP1 in these neuronal cell types impairs mitochondrial fission, causes mitochondrial elongation, and alters apoptotic sensitivity.[9] Thus, CTRP1 may serve as a conserved regulator of mitochondrial dynamics in other cell types, including skeletal muscle.

CTRP1 is a secreted protein belonging to the adiponectin paralog family that has been studied for its systemic metabolic functions. It regulates glucose and lipid catabolism via the AMP-activated protein kinase (AMPK) and insulin receptor substrate 1 (IRS-1) signaling pathways[10,11] and is elevated in the serum of patients with obesity and type 2 diabetes.[12,13] Our previous work demonstrated that CTRP1, which is highly produced in skeletal muscle, elevates blood pressure via vasoconstriction in response to glucocorticoids.[14] However, its intracellular role in skeletal muscles, particularly in mitochondrial regulation, remains poorly understood.

Skeletal muscle regeneration relies on myogenesis, a stepwise process involving satellite cell activation, proliferation, and differentiation. Paired box 7 (Pax7) maintains the satellite cell population, whereas myoblast determination protein 1 (MyoD) and Myogenin sequentially regulate lineage commitment and terminal differentiation.[15] As myofibers mature, the expression of fiber-type-specific genes, such as myosin heavy chain 1 (MyHC1; highly oxidative type I), Myh2 (oxidative type IIA), and Myh4 (glycolytic type IIB), reflects their metabolic profiles.[16] Myogenic differentiation, a key component of this process, requires coordinated metabolic remodeling depending on environmental challenges, in which mitochondrial function influences both lineage progression and fiber-type determination.[4,17] Clinical studies also support this notion, as they show that impaired mitochondrial dynamics are linked to defective differentiation and regeneration.[4,18]

Despite the growing evidence linking mitochondrial dynamics to muscle differentiation and regeneration, the upstream regulators of this process remain incompletely understood. Given its reported role in promoting mitochondrial fission in non-muscle cells,[9] CTRP1 may contribute to skeletal muscle homeostasis by modulating mitochondrial remodeling. In this study, we investigated whether CTRP1 regulates mitochondrial dynamics and promotes myogenic differentiation of skeletal muscle.

RESULTS

CTRP1 is essential for myogenic differentiation in C2C12 cells

Consistent with our previous findings uncovering its role as a myokine,[14] we found that CTRP1 expression was highly enriched in the skeletal muscle compared to other metabolically active tissues, including the liver and white adipose tissue (WAT; Figure 1A), with no detectable age-dependent variation (Figure 1B). Among the various muscles, CTRP1 levels were notably elevated in the skeletal and cardiac muscles compared to those in the smooth muscle tissues (Figure 1C). During myogenic differentiation of C2C12 cells, CTRP1 protein levels progressively increased from the myoblast to myotube stage, without alteration at the transcriptional level (Figure 1D). To assess the functional role of CTRP1 in myogenic differentiation, we depleted CTRP1 in C2C12 myoblasts using guide RNA (gRNA) designed to target the mouse *Ctrp1* genome locus, combined with Cas9 protein (Figure S1). CTRP1 depletion markedly impaired myotube formation without affecting myoblast proliferation (Figure 1E) and was associated with reduced expression of the myogenic transcription factor, myogenin (Figure 1F). Consistently, CTRP1 knockdown or CTRP1 restoration did not alter cell cycle distribution or key regulators (*Cyclin D1*, *Cyclin E1*, and *Cdk 1*), nor the expression of the kinetic marker, Ki67 (Figure S2), supporting a proliferation-independent mechanism. These findings identify CTRP1 as a previously unrecognized essential regulator of skeletal muscle differentiation.

Skeletal muscle-specific CTRP1-knockout mice disrupt skeletal muscle structure and function

To investigate the muscle-intrinsic role of CTRP1 *in vivo*, we generated skeletal muscle-specific CTRP1-knockout (CTRP1 KO$^{\Delta ACTA}$) mice by flanking exon 3 of the *Ctrp1* gene with *loxP* sites (CTRP1$^{fl/fl}$) and crossing them with transgenic (Tg) mice expressing *Cre* recombinase under the human alpha-skeletal actin promoter (ACTA-Cre Tg; Figures 2A and 2B). CTRP1 KO$^{\Delta ACTA}$ mice did not display lethal developmental abnormalities and exhibited similar body weights compared to their CTRP1$^{fl/fl}$ littermate controls (wild type [WT]; Figure 2C), although global KO of CTRP1 showed an embryonic lethal phenotype.[19] However, CTRP1 KO$^{\Delta ACTA}$ mice displayed approximately a 10% reduction in skeletal muscle mass (Figure 2D) and a decreased cross-sectional area (CSA) of the triceps surae muscle (Figure 2E).

Histological analysis of the gastrocnemius muscle revealed myopathic features in CTRP1 KO$^{\Delta ACTA}$ mice, including an increased frequency of enlarged, rounded fibers and a loss of normal polygonal morphology, leading to greater fiber size variability and reduced total fiber number (Figure 2F). Moderate perivascular inflammatory infiltration (indicated by #, Figure 2F) and focal fiber invasion (indicated by *, Figure 2F) were also observed. Immunofluorescence (IF) staining showed a ≈56% reduction in oxidative type IIA fibers and a ≈74% increase in glycolytic type IIB fibers in CTRP1 KO$^{\Delta ACTA}$ muscle, whereas the proportion of type I fibers remained unchanged (Figure 2G).

Extending beyond the triceps surae, we quantified deletion efficiency in individual skeletal muscles. CTRP1 protein and mRNA were reduced in the tibialis anterior (TA), triceps brachii, quadriceps, gastrocnemius, and soleus, whereas the extensor digitorum longus (EDL) showed no significant reduction (Figures S3A and S3B). This exception likely reflects lower and/or more variable Cre

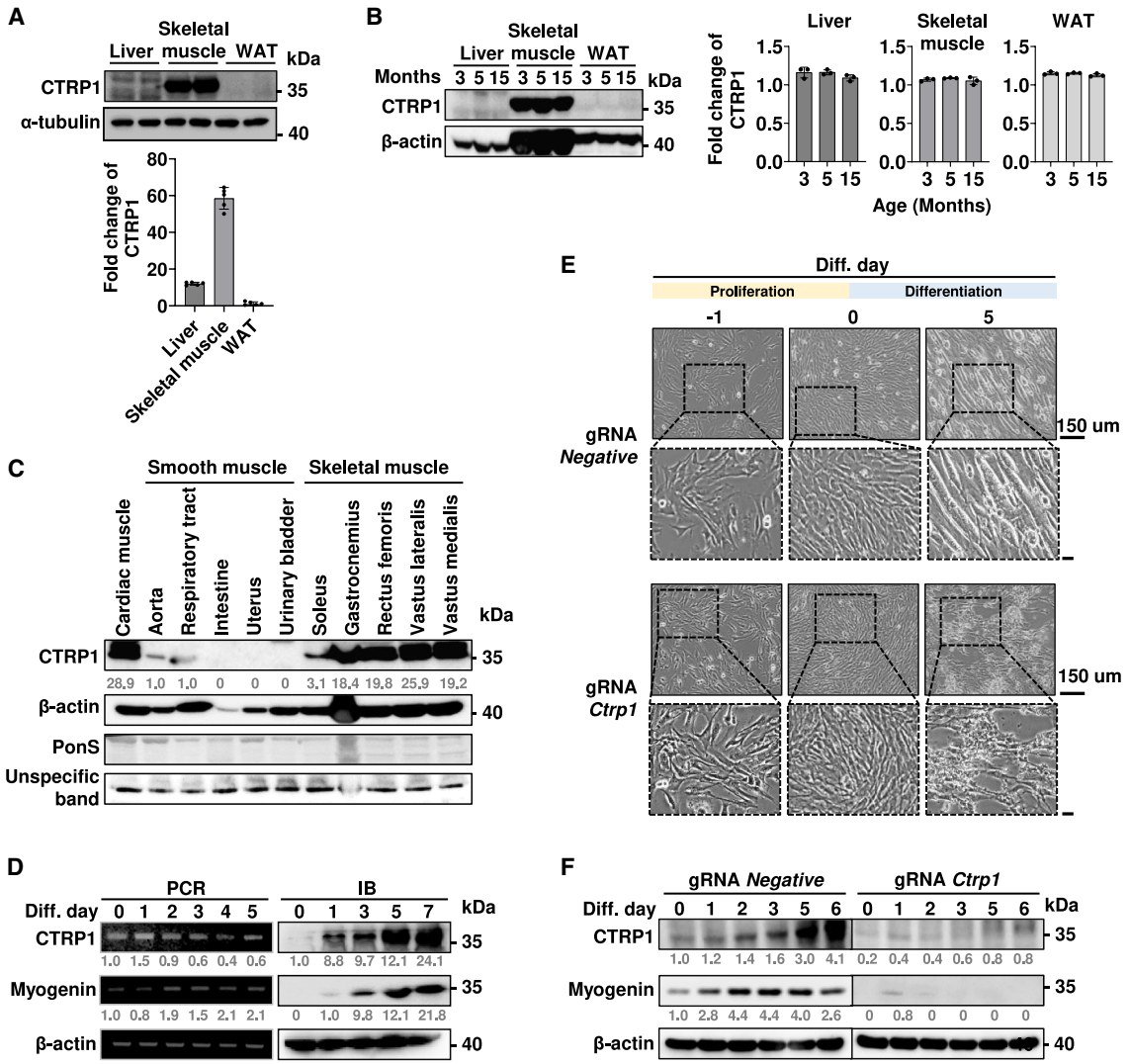


Figure 1. Depletion of CTRP1 impairs myogenic differentiation in C2C12 cells

(A–C) CTRP1 protein levels were analyzed in the indicated tissues from WT mice using immunoblotting. α-tubulin (A), β-actin (B and C), additional PonS staining, and unspecific bands detected by the α-CTRP1 antibody (C) were used as loading controls. Quantification of the CTRP1/α-tubulin ratio (A, bottom), CTRP1/β-actin (B, right), and CTRP1/PonS (C) is shown, with values presented as mean ± SD (A and B) or as digitized numbers (C). (D) Changes in CTRP1 levels during C2C12 differentiation were analyzed using RT-qPCR (left) and immunoblotting (right). Myogenin and CTRP1 levels were normalized and quantified relative to β-actin as the loading control. (E and F) CTRP1 knockdown impairs C2C12 myoblast differentiation. A time-course analysis of myogenic differentiation in control C2C12 (gRNA *negative*) and CTRP1-depleted C2C12 cells (gRNA *Ctrp1*) using the CRISPR-Cas9 system was performed, with representative phase-contrast micrographs of differentiating C2C12 cells captured at days −1, 0, and 5 (E). Time-course analysis of CTRP1 and myogenin protein levels by immunoblotting during C2C12 differentiation (days 0–6) is shown, with levels normalized and quantified using β-actin as the loading control (F). WAT, white adipose tissue; PonS, Ponceau S; Diff, differentiation; gRNA, guide RNA; IB, immunoblotting.

recombinase transgene expression/activity in the EDL. Absolute muscle weights were generally decreased in CTRP1 KO$^{\Delta ACTA}$ mice (Figure S3C), but after normalization to body weight, only the soleus remained significantly lower (Figure S3D). Fiber-type profiles showed trends consistent with those in the triceps surae as type IIA decreased, type IIB increased, and type I changed minimally, indicating a shift toward a more glycolytic, type IIB-like phenotype in CTRP1 KO$^{\Delta ACTA}$ mice (Figure S3E).

In parallel, CTRP1 KO$^{\Delta ACTA}$ muscle exhibited a ≈50% reduction in myogenin protein levels (Figure 2H) and decreased *Myogenin* mRNA expression (Figure 2I), consistent with the impaired myogenic differentiation in CTRP1-depleted C2C12 cells (Figures 1E and 1F). Functionally, CTRP1 KO$^{\Delta ACTA}$ mice exhibited reduced muscle strength compared to WT mice, as evidenced by a shorter latency to fall in the inverted screen test (Figure 2J) and lower grip strength (Figure 2K). These results demonstrate that skeletal

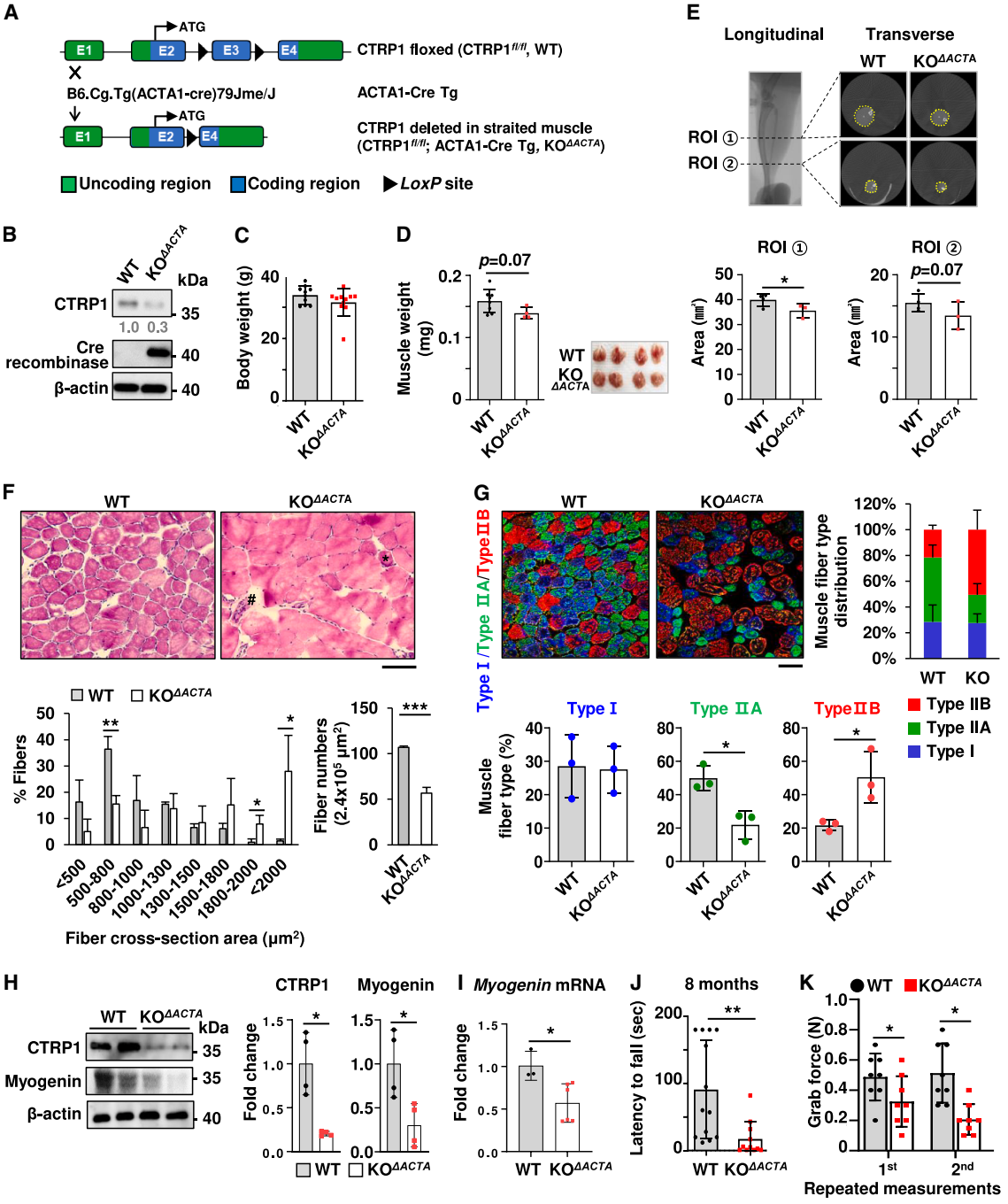


Figure 2. Skeletal muscle-specific CTRP1-knockout mice exhibit a defective muscle phenotype

(A and B) Generation of CTRP1-knockout (CTRP1 KO$^{\Delta ACTA}$) mice. The KO construct is shown (A), and the detailed methods are described in the materials and methods section. CTRP1 and Cre recombinase protein levels were analyzed in the skeletal muscles of WT and CTRP1 KO$^{\Delta ACTA}$ mice and quantified using β-actin as a loading control (B). (C) Body weights of 10-month-old WT and CTRP1 KO$^{\Delta ACTA}$ mice (n = 11–12 per group). (D) Skeletal muscle (triceps surae) weights of 10-month-old WT and CTRP1 KO$^{\Delta ACTA}$ mice (n = 4–8 per group), along with a photograph (right). (E) Micro-CT images of the skeletal muscle from 9-month-old WT and CTRP1 KO$^{\Delta ACTA}$ mice (n = 3–4 per group). Two ROIs within the triceps surae were selected from each mouse, with three-dimensional longitudinal images (top left) reconstructed into two-dimensional images (top right) to evaluate the surface area of the fibula- and tibia-excluded transverse muscle slices (bottom). *$p < 0.05$, two-tailed Student's t test. (F) Representative H&E staining of gastrocnemius muscle cross-sections from 10-month-old WT and CTRP1 KO$^{\Delta ACTA}$ mice, with pathologically altered regions indicated by * and # (top, n = 3–4 per group, scale bar: 50 μm). Quantitative morphometric analysis of muscle fiber size distribution (bottom left) and fiber numbers (bottom right) is presented as mean ± SD.

(legend continued on next page)

CTRP1 is required to maintain muscle size, fiber composition, and functional strength *in vivo*.

CTRP1 is required for cardiotoxin-induced myogenic differentiation *in vivo*

Given that CTRP1 deficiency impairs myogenic differentiation *in vitro*, CTRP1 is likely to play a crucial role in myogenesis during muscle regeneration after cardiotoxin (CTX)-induced injury. Therefore, we assessed CTRP1 levels during injury-associated myogenesis using a CTX-induced muscle injury model. CTRP1 protein expression increased approximately 3.3-fold in the gastrocnemius muscle on day 5 post-CTX injection compared to that in the contralateral vehicle (Veh)-injected muscle (Figure 3A).

Temporal profiling of myogenic markers revealed dysregulation of the regeneration program in CTRP1 KO$^{\Delta ACTA}$ mice. In CTRP1 KO$^{\Delta ACTA}$ mice, *Pax7* mRNA expression, a marker of satellite cells, failed to show the characteristic peak at day 3 and remained low, with only a modest increase by day 7, whereas WT mice exhibited a robust peak at day 3, followed by a return to baseline by day 7 (Figure 3B). Consistent with these transcript data, quantification of Pax7^{+}/DAPI^{+} nuclei per field of muscle area through IF staining showed a similar temporal pattern; however, the magnitude of change in the IF counts was more modest than the reverse transcription quantitative polymerase chain reaction (RT-qPCR) fold changes (Figure S4). Expression of *MyoD*, *Myh2*, and *Myh4* mRNAs, which are essential for myogenic differentiation, was dysregulated in CTRP1 KO$^{\Delta ACTA}$ mice: *MyoD* and *Myh2* mRNA expression levels were delayed and attenuated compared to the robust induction observed in WT mice (Figures 3C and 3D), whereas *Myh4* mRNA, which was elevated at baseline, failed to respond to CTX-induced injury in CTRP1 KO$^{\Delta ACTA}$ mice (Figure 3E). The expression of muscle atrophy markers, *MaFbx* and *Murf1* mRNA, increased at baseline but failed to fluctuate with CTX-induced injury in CTRP1-KO mice (Figures 3F and 3G).

Histological analysis of CTX-injured muscle revealed a reduction in the total number of fibers in CTRP1 KO$^{\Delta ACTA}$ mice, accompanied by increased necrotic and hypereosinophilic fibers (Figure 3H). These pathological features are consistent with delayed myogenic progression and impaired structural remodeling following injury in CTRP1 KO$^{\Delta ACTA}$ mice.

To assess whether impaired regeneration was intrinsic to myogenic cells, primary myoblasts were isolated from CTRP1 KO$^{\Delta ACTA}$ mice and induced to differentiate *ex vivo*. CTRP1 KO$^{\Delta ACTA}$ myoblasts exhibited impaired myotube formation (Figure 3I) and significantly reduced mRNA expression of *MyoD*, *myogenin*, *Myh4*, and *Myh2*, whereas the expression of the muscle atrophy gene *MaFbx* was unaffected (Figure 3J), confirming the direct role of CTRP1 in regulating myogenic differentiation.

CTRP1 restoration rescues mitochondrial function and myogenic differentiation of CTRP1 KO$^{\Delta ACTA}$ myoblasts

Given the critical role of mitochondria in myogenic differentiation, we investigated whether CTRP1 modulates mitochondrial function. In CTRP1 KO$^{\Delta ACTA}$ myotubes, the protein levels of key mitochondrial markers, including uncoupling protein 1 (UCP1) and cytochrome *c* oxidase subunit 4 (COX IV), were reduced by approximately 40%, coinciding with a marked decrease in myogenin expression, which is a key regulator of myogenic differentiation (Figure 4A). Consistent with this, the mitochondrial membrane potential, assessed by tetramethylrhodamine ethyl ester (TMRE) staining, was substantially diminished in CTRP1 KO$^{\Delta ACTA}$ myotubes, which also exhibited thinner and less mature myotube structures (Figure 4B). Conversely, transient overexpression of CTRP1 in C2C12 myoblasts significantly enhanced the mitochondrial membrane potential (Figure 4C), supporting the positive regulatory role of CTRP1 in mitochondrial function.

To further characterize the functional impact of CTRP1 loss, we performed extracellular flux analysis. Undifferentiated myoblasts were used to exclude the possibility that mitochondrial dysfunction was a secondary effect of impaired myogenic differentiation. This analysis revealed that CTRP1 deficiency impairs mitochondrial respiration. While the basal oxygen consumption rate (OCR) was largely unaffected, both maximal respiration and spare respiratory capacity (SRC) were significantly decreased in CTRP1 KO$^{\Delta ACTA}$ myoblasts, indicating compromised mitochondrial adaptability (Figure 4D). These defects were rescued upon reintroduction of CTRP1 via adenoviral delivery (AD*ctrp1*), restoring both maximal respiration and the SRC (Figure 4D).

Consistently, COX IV activity was also reduced in CTRP1 KO$^{\Delta ACTA}$ myoblasts, reflecting the decrease in protein expression, and was partially restored by AD*ctrp1* (Figure 4E). AD*ctrp1* not only rescued mitochondrial function but also restored myogenic differentiation, as indicated by the recovery of mRNA expression levels of *MyoD*, *Myh4*, and *Myh2* (Figure 4F, top). Meanwhile, AD*ctrp1* increased

$^{*}p < 0.05$ and $^{**}p < 0.01$, two-tailed Student's *t* test. (G) Representative immunofluorescence (IF) staining of gastrocnemius muscle cross-sections from 11-month-old WT and KO mice to identify fiber types (top left, $n = 3$ per group, scale bar: 40 μm), along with fiber-type frequency data (top right and bottom). Values are presented as mean ± SD. $^{*}p < 0.05$, two-tailed Student's *t* test. (H) CTRP1 and myogenin protein levels were analyzed by immunoblotting in the triceps surae of 11-month-old WT and KO mice (left, $n = 4$ per group) and normalized using β-actin as a loading control (right). Values are presented as mean ± SD. $^{*}p < 0.05$ and $^{**}p < 0.01$, two-tailed Student's *t* test. (I) *Myogenin* mRNA levels in the triceps surae of 11-month-old WT and CTRP1 KO$^{\Delta ACTA}$ mice were analyzed using RT-qPCR and normalized using β-actin as a loading control ($n = 3$–6 per group). Values are presented as mean ± SD. $^{*}p < 0.05$, two-tailed Student's *t* test. (J and K) Motor ability assessments of CTRP1 KO$^{\Delta ACTA}$ mice. Latency to fall on the inverted screen in 9-month-old WT and CTRP1 KO$^{\Delta ACTA}$ mice (J, $n = 9$–13 per group) and grip strength tests performed weekly in 10- to 11-month-old WT and CTRP1 KO$^{\Delta ACTA}$ mice (K, $n = 8$ per group). Values are presented as mean ± SD. $^{*}p < 0.05$ and $^{**}p < 0.01$, Tukey's test. Fl, floxed; WT, wild-type mouse; Tg, transgenic mouse; KO, knockout mouse; ROI, region of interest.

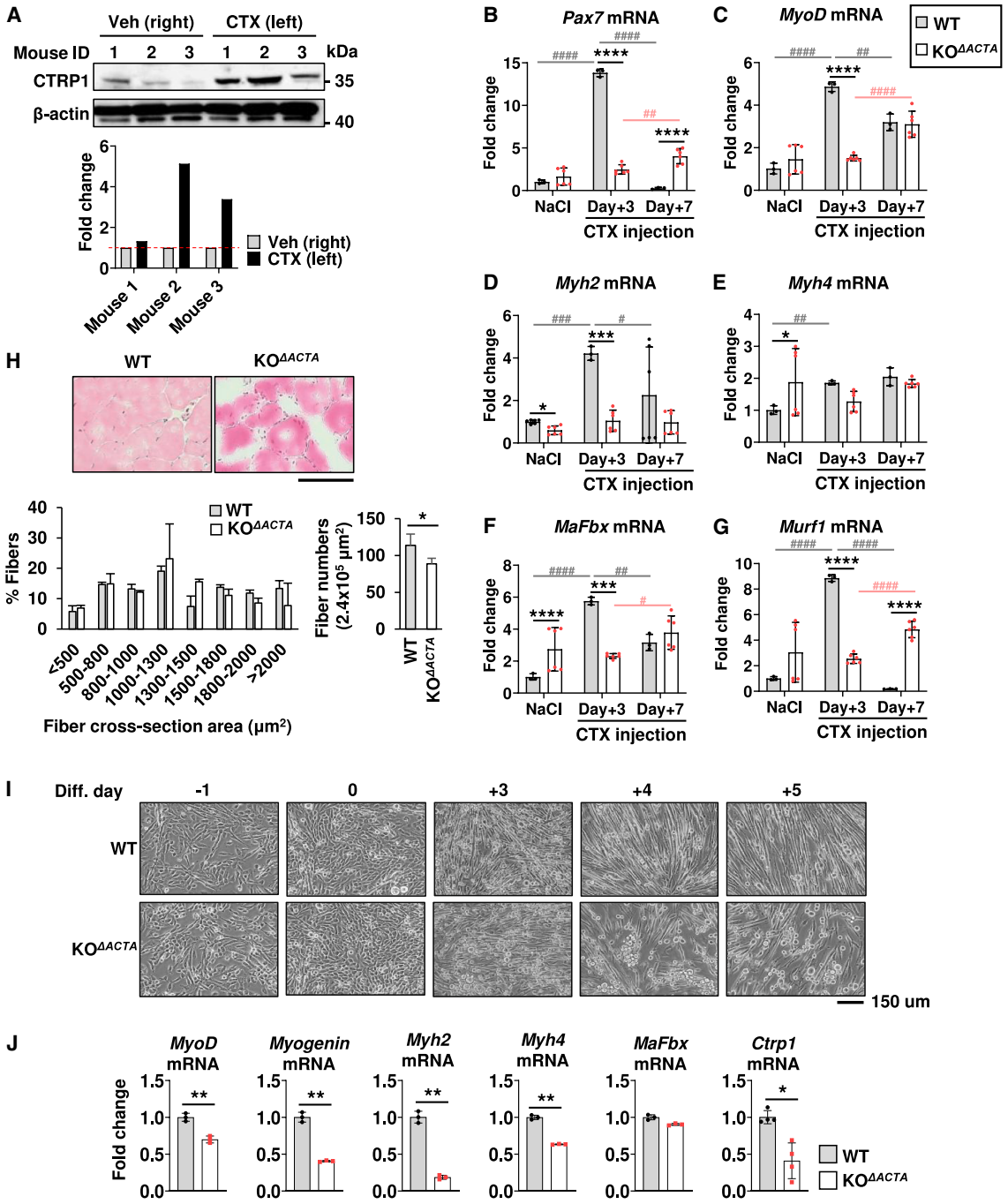


Figure 3. CTRP1 KO$^{\Delta ACTA}$ mice exhibit impaired muscle regeneration after CTX injury and disrupted myogenic differentiation, which is rescued by CTRP1 restoration

(A) CTRP1 protein levels were analyzed by immunoblotting in the triceps surae of 7-week-old WT mice 5 days after injection with 10 μM CTX (top, $n = 3$). CTRP1 protein levels in the CTX-injected gastrocnemius muscle (left hindlimb) were compared with those in the contralateral control gastrocnemius muscle injected with the vehicle alone (right hindlimb) and normalized using β-actin as a loading control (bottom). Values are presented as mean ± SD. *$p < 0.05$, two-tailed Student's t test. (B–H) Molecular and morphological changes in the regenerating triceps surae muscle post-injury in 10-month-old WT and CTRP1 KO$^{\Delta ACTA}$ mice. NaCl was used as the vehicle control ($n = 3$–6). Myogenic gene levels were assessed using RT-qPCR at the indicated days post-CTX injection. β-actin was used as a loading control. Values are presented as the mean ± SD. * indicates significant differences between WT and CTRP1 KO$^{\Delta ACTA}$ mice on the same post-CTX injection day, whereas # indicates significant differences between post-CTX injection days within the same genotype. * or #$p < 0.05$, ** or ##$p < 0.01$, *** or ###$p < 0.001$, and **** or ####$p < 0.001$, Tukey's test (B–G). Histological analysis of the

(legend continued on next page)

Ctrp1 mRNA (Figure 4F, bottom) and CTRP1 protein (Figure 4G) by 1.5×10^3-fold and 4.5-fold versus CTRP1 KO$^{\Delta ACTA}$+AD*gfp*, respectively. Collectively, these findings suggest that CTRP1 is essential for maintaining mitochondrial functional capacity, particularly respiratory efficiency and membrane potential, supporting proper myogenic differentiation.

CTRP1 deficiency leads to DRP1-engaged mitochondrial defects in skeletal muscle

As cristae density serves as an ultrastructural indicator of the mitochondrial membrane potential,[20] we performed transmission electron microscopy (TEM) to examine the cristae structure in CTRP1 KO$^{\Delta ACTA}$ skeletal muscles. Interestingly, intermyofibrillar (IMF) mitochondria showed an abnormal reduction in cristae density (Figures 5A and 5B), consistent with an impaired mitochondrial membrane potential.

CTRP1 KO$^{\Delta ACTA}$ skeletal muscle also exhibited abnormally elongated mitochondria (Figure 5A), accompanied by a significant reduction in the total mitochondrial area (Figure 5C), whereas the number of mitochondria remained unchanged (Figure 5D). These structural abnormalities coincided with a reduced mitochondrial DNA (mtDNA) content in the CTRP1 KO$^{\Delta ACTA}$ muscle (Figure 5E). To further explore the molecular mechanism underlying mitochondrial elongation, we examined the subcellular localization of DRP1, a key mediator of mitochondrial fission that has been reported to physically interact with CTRP1 and is essential for proper mitochondrial fission.[9] In the mitochondrial fraction of CTRP1 KO$^{\Delta ACTA}$ skeletal muscle, DRP1 levels were markedly reduced, whereas cytosolic DRP1 levels remained unchanged (Figure 5F). Consistently, IF analysis revealed a significant reduction in the colocalization of DRP1 and mitochondria in the CTRP1 KO$^{\Delta ACTA}$ skeletal muscle (Figure 5G). Collectively, the abnormal mitochondrial elongation observed in CTRP1 KO$^{\Delta ACTA}$ skeletal muscle is likely due to impaired DRP1 recruitment to the mitochondria.

CTRP1-enriched mitochondria restored myogenic differentiation in CTRP1 KO$^{\Delta ACTA}$ myoblasts

To further prove whether CTRP1 promotes myogenic differentiation through a mitochondria-dependent mechanism, we conducted both direct gene expression rescue and mitochondrial transplantation experiments in CTRP1 KO$^{\Delta ACTA}$ myoblasts. As shown in Figure 6A, CTRP1 KO$^{\Delta ACTA}$ myoblasts were transduced with adenoviral CTRP1 (AD*ctrp1*) to restore CTRP1 expression or were treated with mitochondria isolated from AD*ctrp1*-infected CTRP1 KO$^{\Delta ACTA}$ myoblasts (mito$^{AD ctrp1}$). In both cases, restoration of CTRP1 function led to a substantial recovery of the mitochondrial membrane potential and enhanced myotube formation (Figures 6B and 6C).

Transplantation of mitochondria from GFP-infected control myoblasts (mito$^{AD gfp}$) into CTRP1 KO$^{\Delta ACTA}$ myoblasts led to an increase in mitochondrial mass but failed to restore mitochondrial potential, myotube formation, or the expression of key myogenic markers (Figures 6B and 6C). Together, these results demonstrate that CTRP1 is a critical regulator of myogenic differentiation, acting through the modulation of mitochondrial function, and that CTRP1-conditioned mitochondria are sufficient to rescue the myogenic defects in CTRP1 KO$^{\Delta ACTA}$ myoblasts.

CTRP1 expression is diminished in human myopathy

To evaluate the clinical relevance of CTRP1, we examined skeletal muscle biopsies obtained from patients diagnosed with polymyositis (PM), dermatomyositis (DM), or Duchenne muscular dystrophy (DMD). Compared to healthy controls, CTRP1 expression was significantly reduced in all patient groups and progressively decreased in accordance with disease severity in both DM and DMD (Figure 7A). In healthy muscle tissue, CTRP1 was predominantly localized to the endomysium, surrounding but not within the muscle fibers (Figure 7B). In contrast, myopathy samples exhibited altered CTRP1 localization and ectopic accumulation, often in regions showing histological signs of sterile inflammation and fiber degeneration (Figure 7B).

To broaden clinical insights and address the limitations of a small patient cohort, *in silico* analysis of a public dataset (GEO: GSE3307) confirmed significant downregulation of *Ctrp1* mRNA in the skeletal muscle of patients with acute quadriplegic myopathy, juvenile DM, and amyotrophic lateral sclerosis compared to healthy controls (Figure 7C). Although these human diseases were not directly modeled in our mouse studies, the consistent reduction in CTRP1 expression across multiple myopathies, combined with functional evidence from genetic and cellular models, suggests that CTRP1 deficiency contributes to skeletal muscle defects and mitochondrial dysfunction in disease. These results support the potential of CTRP1 as an evidence-based biomarker of myogenic dysfunction and a candidate for therapeutic intervention in myopathies.

DISCUSSION

CTRP1, a member of the CTRP family, is highly expressed in skeletal muscle; however, its function in this tissue remains largely uncharacterized. In this study, we identified CTRP1 as a key regulator of muscle differentiation and regeneration. CRISPR-Cas9-mediated deletion of CTRP1 in C2C12 myoblasts impaired myogenic

regenerating gastrocnemius muscle in CTRP1 KO$^{\Delta ACTA}$ mice 7 days post-injury (H). Representative H&E staining of gastrocnemius muscle cross-sections (top, scale bar: 40 μm) and quantitative morphometric evaluation of muscle fiber size distribution (bottom left) and fiber numbers (bottom right) are shown. Values are presented as mean ± SD. *$p < 0.05$, two-tailed Student's *t* test. (I and J) Primary myoblasts from 7-month-old WT and CTRP1 KO$^{\Delta ACTA}$ mice were differentiated into myotubes. Representative phase-contrast images ($n = 6–7$) are shown (I). Five days post-differentiation initiation, cells were analyzed by RT-qPCR for myogenic gene expression, and relative myogenic gene levels were normalized to β-actin as a loading control (J). Veh, vehicle; CTX, cardiotoxin; WT, wild type; KO, knockout; Diff, differentiation.

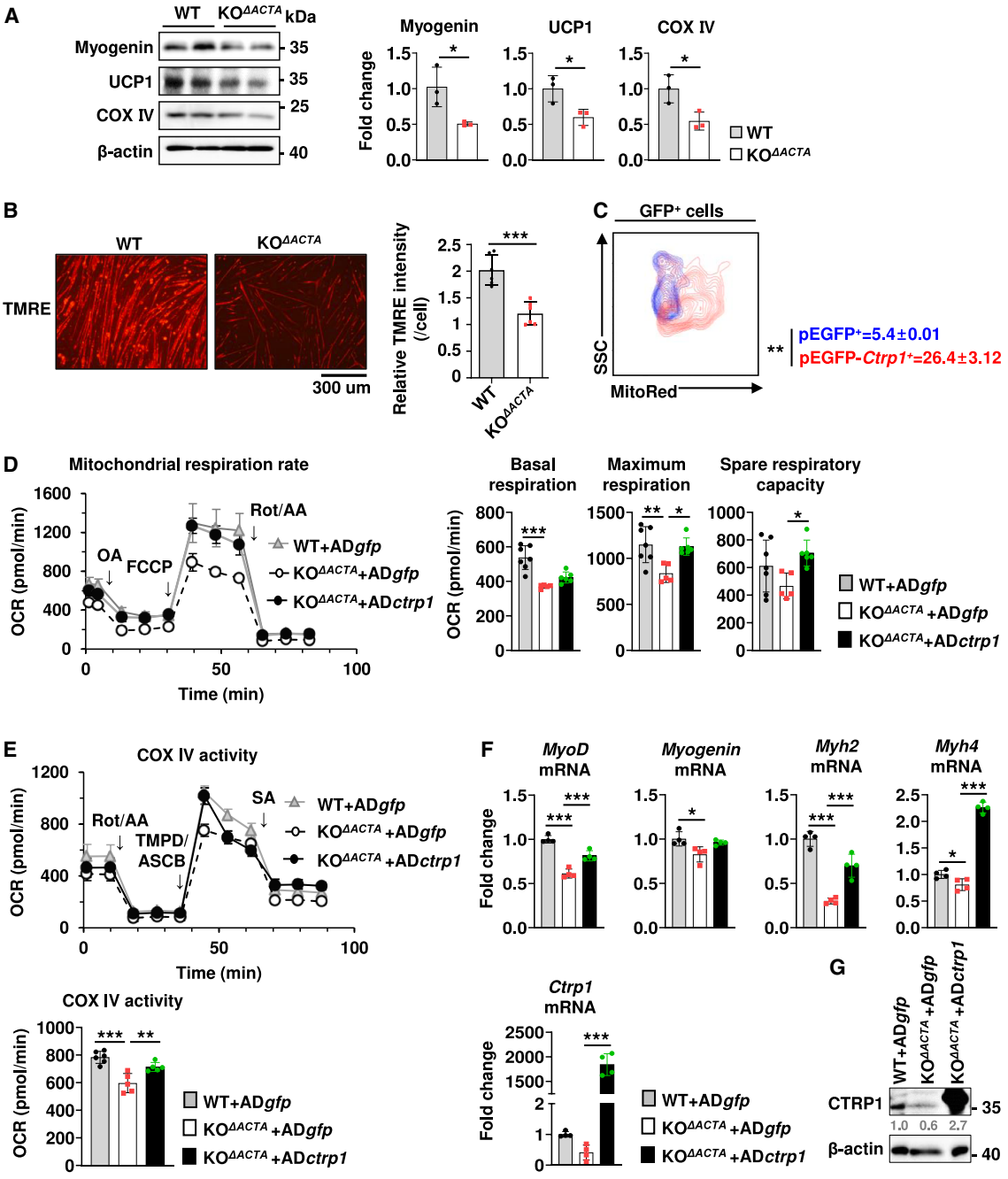


Figure 4. CTRP1 enhances mitochondrial function

(A) Primary myoblasts from 7-month-old WT and CTRP1 KO$^{\Delta ACTA}$ mice were differentiated into myotubes. Five days post-differentiation initiation, cells were analyzed, and mitochondrial protein levels were analyzed by immunoblotting (A, left) and normalized to β-actin (A, right). Values are presented as mean ± SD. *$p < 0.05$, two-tailed Student's *t* test. (B) Differentiated cells were stained with TMRE to assess the mitochondrial membrane potential in live cells (left), and TMRE fluorescence intensity was measured and quantified (right). Values are presented as mean ± SD. ***$p < 0.001$, two-tailed Student's *t* test. (C) Changes in the MitoRed-positive cell population in CTRP1-overexpressing C2C12 myoblasts were determined by flow cytometry. The pEGFP empty plasmid was used as a mock control. The population of MitoRed-positive cells among GPF-positive cells was quantified and expressed as a percentage. Values are presented as mean ± SD. **$p < 0.01$, two-tailed Student's *t* test. (D–G) Adenovirus-mediated recovery of CTRP1 restores mitochondrial function and myogenesis in CTRP1-KO myoblasts. Primary myoblasts isolated from 7-month-old WT and CTRP1 KO$^{\Delta ACTA}$ mice ($n = 3$) were infected with adenoviruses encoding GFP (AD*gfp*) and/or CTRP1 (AD*ctrp1*) for 18 h. The OCR (D) and COX IV activity (E) were measured, and detailed methods are described

(legend continued on next page)

differentiation into myotubes, and muscle-specific CTRP1-KO mice (CTRP1 KO$^{\Delta ACTA}$) exhibited reduced muscle mass, decreased function, and a fiber-type shift from oxidative type IIA to glycolytic type IIB fibers. To extend our findings at the transcriptomic level, we performed RNA sequencing (RNA-seq) of the triceps surae from WT and CTRP1 KO$^{\Delta ACTA}$ mice. Principal-component analysis (PCA) separated the genotypes and identified 322 downregulated and 180 upregulated differentially expressed genes (DEGs) (Figures S5A–S5C). Fiber-type gene analysis showed broad decreases in type I genes (*Atp2a2*, *Myh7b*, *Myh6*, and *Tpm3*) and an overall induction of type IIB genes, indicating a shift toward a more glycolytic program in CTRP1 KO$^{\Delta ACTA}$ muscle (Figure S5D). Gene Ontology (GO) analysis further revealed upregulation of ion-handling/excitability, polyamine/S-adenosylmethionine metabolism, and stress/inflammatory and pro-apoptotic pathways (Figure S5E), with downregulation of muscle contraction/myofibrillar organization, oxidative phosphorylation, ATP metabolism, myotube differentiation, and fast-slow fiber transition (Figures S5F and S6). These findings suggest that CTRP1 contributes to myoblast differentiation and the maintenance of oxidative muscle identity and endurance-related properties. Furthermore, CTRP1 expression progressively increased during CTX-induced muscle regeneration, and the expression of myogenic markers such as *Pax7*, *Myh2*, and *Myh4* mRNA was altered in CTRP1 KO$^{\Delta ACTA}$ mice, indicating CTRP1's critical role in muscle repair.

During myogenesis, myoblasts undergo a metabolic shift tightly coupled to mitochondrial remodeling, including changes in the fusion-fission balance, cristae structure, biogenesis, and mitophagy.[21] CTRP1 deletion severely disrupted mitochondrial function, including loss of membrane potential and impaired oxidative respiration. Restoration of CTRP1 rescued these defects, and transplantation of mitochondria from CTRP1-restored myoblasts into CTRP1 KO$^{\Delta ACTA}$ myoblasts significantly improved mitochondrial function and differentiation capacity. These findings demonstrate that CTRP1 maintains mitochondrial integrity to support effective myogenic differentiation.

To investigate the underlying mechanism, we examined the relationship between CTRP1 and mitochondrial dynamics. We previously showed that CTRP1 localizes to the ER membrane and contributes to mitochondrial fission through its interaction with the fission factor DRP1.[9] In this study, DRP1 levels were markedly reduced in the mitochondrial fraction of CTRP1 KO$^{\Delta ACTA}$ muscle, indicating a defect in DRP1 recruitment. Besides enabling metabolic adaptation, mitochondrial fission plays a critical role in clearing damaged mitochondria via mitophagy, particularly through the PINK1/Parkin pathway.[22] Failure of fission in CTRP1-deficient muscle likely disrupts this process, leading to accumulation of dysfunctional mitochondria, reduced ATP production, and elevated reactive oxygen species (ROS) levels, which contribute to muscle dysfunction and degeneration.[23] Notably, intersection with MitoCarta 3.0 highlighted nine mitochondrial DEGs (Figure S7A) in CTRP1 KO$^{\Delta ACTA}$ muscle, including downregulation of *Pdk4* and *Ak4* and upregulation of *Mthfd1l* (Figure S7B), a pattern consistent with attenuated mitochondrial quality control accompanied by compensatory one-carbon metabolic rerouting. Future studies will directly quantify mitophagy flux *in vivo* and determine whether restoring *PDK*/*AK4* or modulating *Mthfd1l* normalizes mitochondrial turnover and improves muscle function in CTRP1 KO$^{\Delta ACTA}$ mice.

Consistent with these findings, CTRP1 deficiency reduces *Pax7* mRNA expression, which is a master regulator of satellite cell maintenance and myogenic initiation.[24] This suggests that CTRP1 not only regulates mitochondrial function but may also influence muscle stem cell fate through mitochondria-dependent signaling pathways. The concurrent reduction in DRP1-mediated fission and *Pax7* mRNA expression implies a novel axis through which CTRP1 coordinates mitochondrial remodeling and transcriptional regulation during muscle regeneration.

Clinically, we found that CTRP1 expression was significantly decreased in the skeletal muscles of patients with PM, DM, and DMD, which are characterized by chronic inflammation, mitochondrial dysfunction, and regenerative failure. Mitochondrial abnormalities have been widely reported in these myopathies,[3,25] and a recent study demonstrated that mitochondrial transplantation improves differentiation and mitochondrial activity in myoblasts derived from patients with idiopathic inflammatory myopathy (IIM).[18] Given the well-established interplay between mitochondrial dysfunction and chronic inflammation in muscle diseases,[3,25] impaired mitochondrial quality may contribute to an inflammatory milieu, and vice versa. Although we did not directly examine immune signaling, previous studies have implicated CTRP1 in inflammatory pathways,[26] and our findings suggest that CTRP1 may serve as both a target and modulator of the immune-metabolic axis in diseased muscle.

Emerging evidence indicates that impaired myogenesis is a shared mechanism in both inflammatory and genetic myopathies.[27] In PM and DM, mitochondrial dysfunction in the perifascicular regions correlates with reduced satellite cell activity, downregulation of mitochondrial regulators such as mitochondrial transcription factor A (TFAM) and PPARGC1A, and increased oxidative stress.[28] Similarly, in DMD, loss of dystrophin leads to profound mitochondrial defects that further impair differentiation and accelerate disease progression.[29] Notably, *in silico* analyses confirmed reduced muscular *Ctrp1* mRNA expression across multiple myopathies, but this

in the materials and methods section. Primary myoblasts were differentiated into mature myotubes, and 5 days post-differentiation, the cells were lysed to analyze myogenic gene levels by RT-qPCR and normalized using β-actin as a loading control (F). CTRP1 protein levels were analyzed using immunoblotting, and the quantification of the CTRP1/β-actin ratio (B, right) is presented as digitized numbers (G). Values are presented as mean ± SD. $^{*}p < 0.05$, $^{**}p < 0.01$, and $^{***}p < 0.001$, Tukey's test. WT, wild-type mouse; KO, knockout mouse; SSC, side scatter; MitoRed, MitoTracker Red.

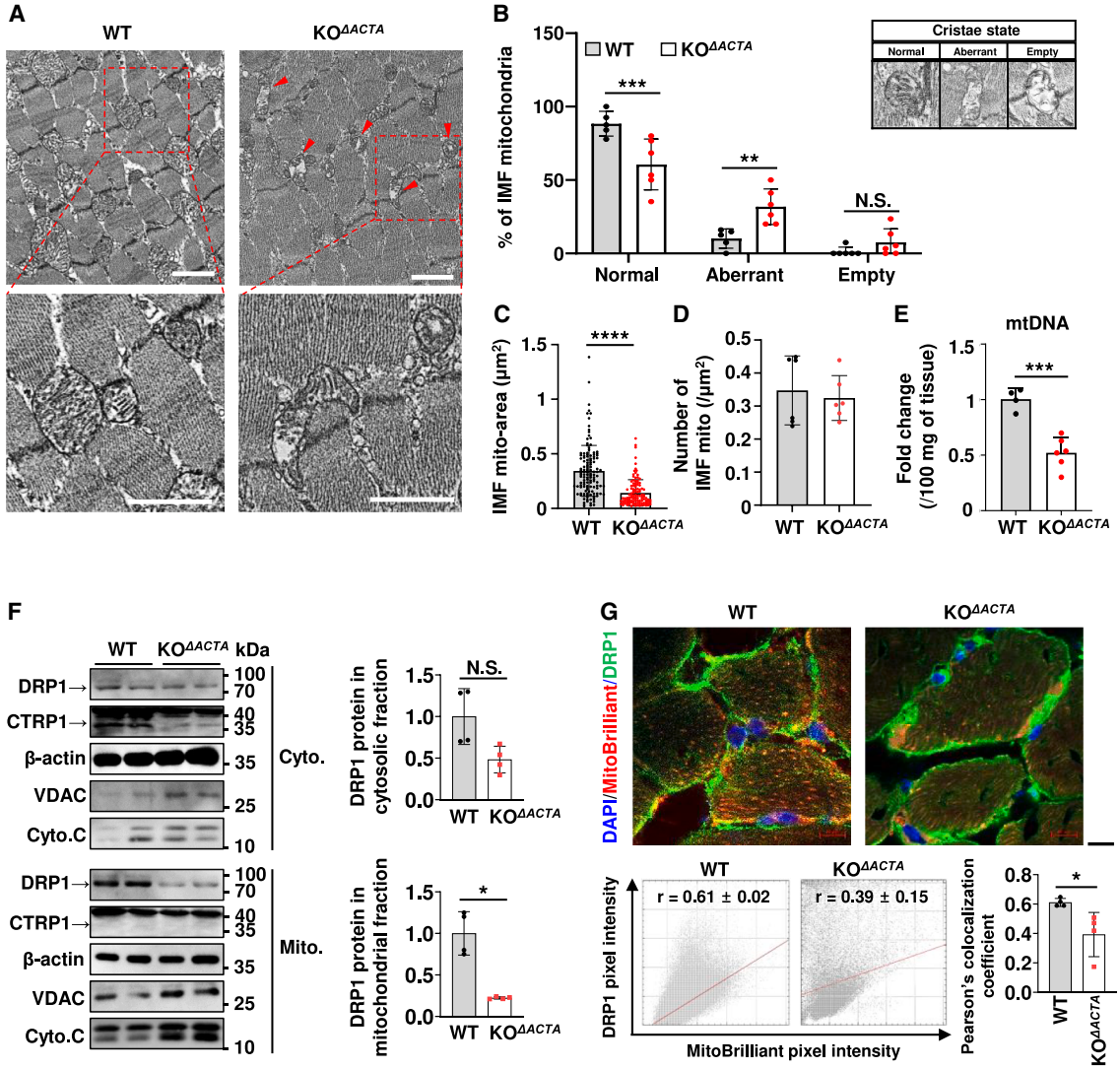


Figure 5. CTRP deficiency leads to DRP1-engaged mitochondrial defects

(A–D) Representative TEM images are shown, with arrows indicating structurally impaired intermyofibrillar (IMF) mitochondria of 10-month-old WT and CTRP1 KO$^{\Delta ACTA}$ mice (n = 3 per group). Regions of interest (ROIs) are boxed and shown as magnified images (A, scale bar: 1 μm). The state of cristae in the IMF mitochondria (B), mean area of the IMF mitochondria (C), and number of IMF mitochondria per 1 μm^2 (D) were measured and quantified from the TEM images. Values are presented as mean ± SD. N.S., not significant; $^{**}p < 0.01$, $^{***}p < 0.001$, and $^{****}p < 0.0001$, two-tailed Student's t test. (E) Relative mtDNA content from the triceps surae of 7-month-old WT and CTRP1 KO$^{\Delta ACTA}$ mice (n = 4–6) was determined by RT-qPCR analysis of NADH dehydrogenase subunit 1 (mtDNA), normalized to Lpl (genomic DNA). Values are presented as mean ± SD. $^{***}p < 0.001$, two-tailed Student's t test. (F) Triceps surae muscles from 10-month-old WT and CTRP1 KO$^{\Delta ACTA}$ mice were used to prepare the cytosolic and mitochondrial fractions. DRP1 and CTRP1 protein levels were analyzed using immunoblotting. β-actin, VDAC, and cytochrome c (Cyto. C) were used as loading controls for the cytosolic and mitochondrial fractions, respectively (left). Quantification of the DRP1/β-actin and DRP1/VDAC ratios for DRP1 localization is shown (right). Values are presented as mean ± SD. N.S., not significant; $^{*}p < 0.05$, two-tailed Student's t test. (G) Immunofluorescence staining of endogenous DRP1 and CTRP1 in representative gastrocnemius sections (top), and Pearson's colocalization coefficient (r) was calculated to determine colocalization efficiency between CTRP1 and DRP1 (bottom) from 10-month-old WT and CTRP1 KO$^{\Delta ACTA}$ mice (n = 4 per group). DAPI was used to counterstain the DNA in immunofluorescence images. Scale bar: 10 μm. Values are presented as mean ± SD. N.S., not significant; $^{*}p < 0.05$, two-tailed Student's t test. WT, wild-type mouse; KO, knockout mouse; mtDNA, mitochondrial DNA; Cyto, cytosolic fraction; Mito, mitochondrial fraction.

downregulation was pronounced in conditions where mitochondrial dysfunction is a central pathogenic mechanism, such as acute quadriplegic myopathy, juvenile DM, and amyotrophic lateral sclerosis (Table 1). This pattern suggests that CTRP1 may play a functional role in myopathies in which mitochondria contribute directly to disease pathogenesis.

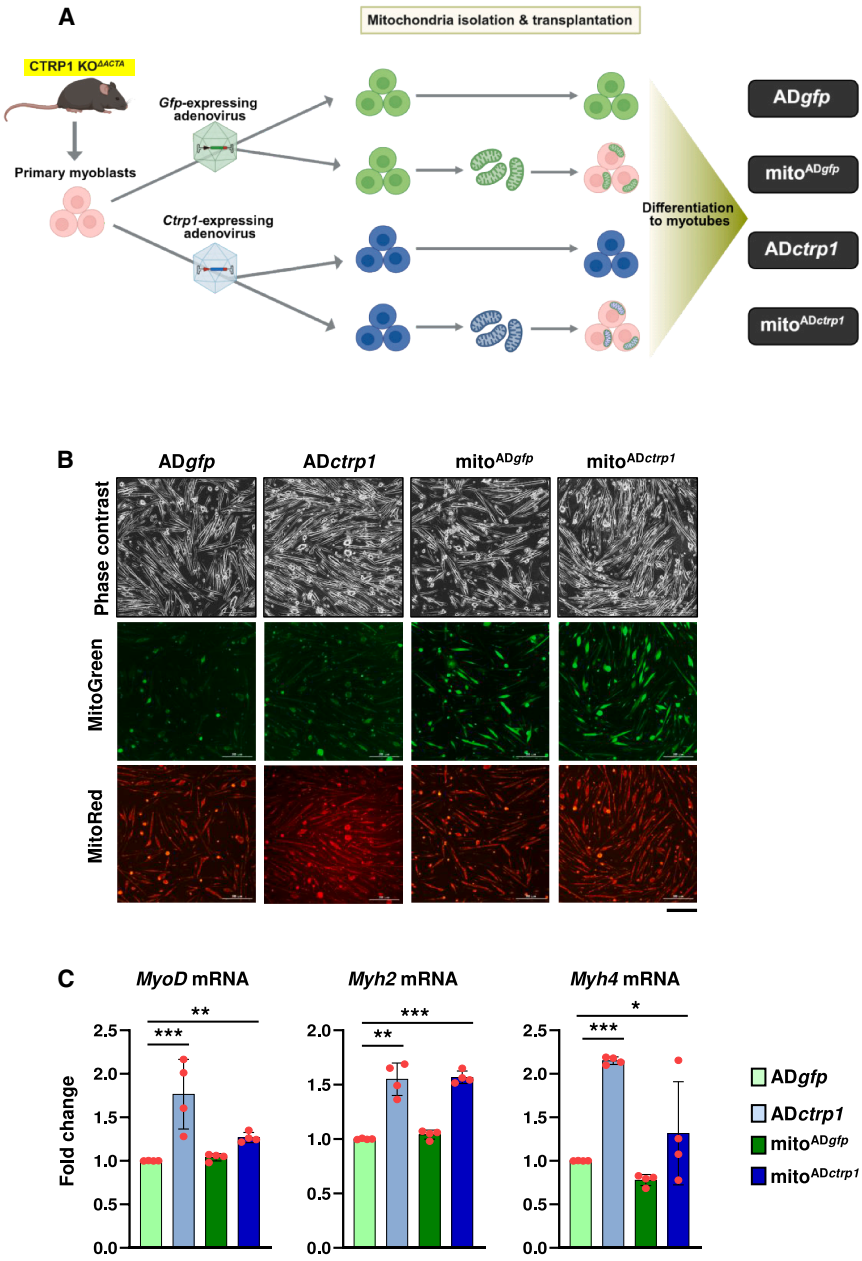


Figure 6. CTRP1 recovery promotes myogenic differentiation by restoring mitochondrial function, as demonstrated by mitochondrial transplantation

(A–C) Mitochondrial transplantation demonstrated that mitochondria are the primary mediators of CTRP1's effects on myogenesis. Experimental design (A): primary myoblasts (PriMUS) were isolated from 7-month-old CTRP1 KO$^{\Delta ACTA}$ mice and infected with adenovirus encoding GFP (AD*gfp*) and/or CTRP1 (AD*ctrp1*) for 18 h. These cells were differentiated into myotubes (indicated as AD*gfp* and/or AD*ctrp1*), or mitochondria were isolated from each infected myoblast. Isolated mitochondria from AD*gfp*- and/or AD*ctrp1*-infected myoblasts were transplanted via mitochondrial uptake into primary CTRP1 KO$^{\Delta ACTA}$ myoblasts, which were then differentiated into myotubes (indicated as mito^{ADgfp} and/or mito^{ADctrp1}). The experimental design was created using BioRender.com. After 5 days of differentiation, the cells were stained with MitoTracker Green (MitoGreen) to assess mitochondrial mass and MitoTracker Red (MitoRed) to assess mitochondrial potential, and myotube formation and fluorescence intensity were observed. Scale bar: 150 μm (B). After 5 days of differentiation, the cells were lysed, and myogenic gene levels were analyzed by RT-qPCR and normalized using β-actin as a loading control. Values are presented as mean ± SD (C). $^{**}p < 0.01$ and $^{***}p < 0.001$, two-tailed Student's *t* test. KO, knockout mouse.

Downregulation of autophagy and mitophagy is implicated in the pathogenesis of DMD and several limb-girdle muscular dystrophies (LGMDs). Consistent with this, RNA-seq of CTRP1 KO$^{\Delta ACTA}$ muscle showed a coordinated decrease in autophagy/mitophagy-associated transcripts (*Spata33*, *Depp1*, *Sesn3*, *Sesn1*, *Atp2a2*, *Wdfy4*, and *Hap1*) (Figure S7C) together with a MitoCarta overlap highlighting nine mitochondrial DEGs (*Pdk4*, *Ak4*, and *Mthfd1l*) (Figures S7A and S7B). These findings suggest that CTRP1 supports stress-responsive mitochondrial quality control and that loss of CTRP1 likely blunts autophagy/mitophagy, limits cellular adaptation to stress, and may thereby exacerbate disease progression and severity.

To address primary mitochondrial myopathies, we reanalyzed public datasets (GEO: GSE1462 and GSE43698), which did not show significant differences in muscular *Ctrp1* mRNA expression compared to healthy controls, while DMD still demonstrates a pronounced reduction (Figures S8A and S8B). These findings likely reflect the limitations inherent to small sample size and biopsy-site heterogeneity but indicate that reduced CTRP1 expression can occur in a subset of mitochondrial myopathies. Consistent with reviews of ClinVar (https://www.ncbi.nlm.nih.gov/clinvar/) and ClinGen (https://www.ncbi.nlm.nih.gov/clinvar/docs/clingen/) databases, no pathogenic germline variants in the *Ctrp1* gene (*C1qtnf1*) have been significantly associated with disease, supporting the interpretation that downregulation of the *Ctrp1* gene in myopathies is likely secondary to primary genetic lesions but may nonetheless modify disease severity. These findings support the consideration that CTRP1 is both a novel perspective biomarker and a potential therapeutic target, especially in conditions where mitochondrial dysfunction is a prominent feature.

CTRP1 expression increased during brown adipocyte differentiation (Figure S9A) and was enriched in brown adipose tissue (BAT) relative to most WAT depots (Figure S9B), whereas its expression

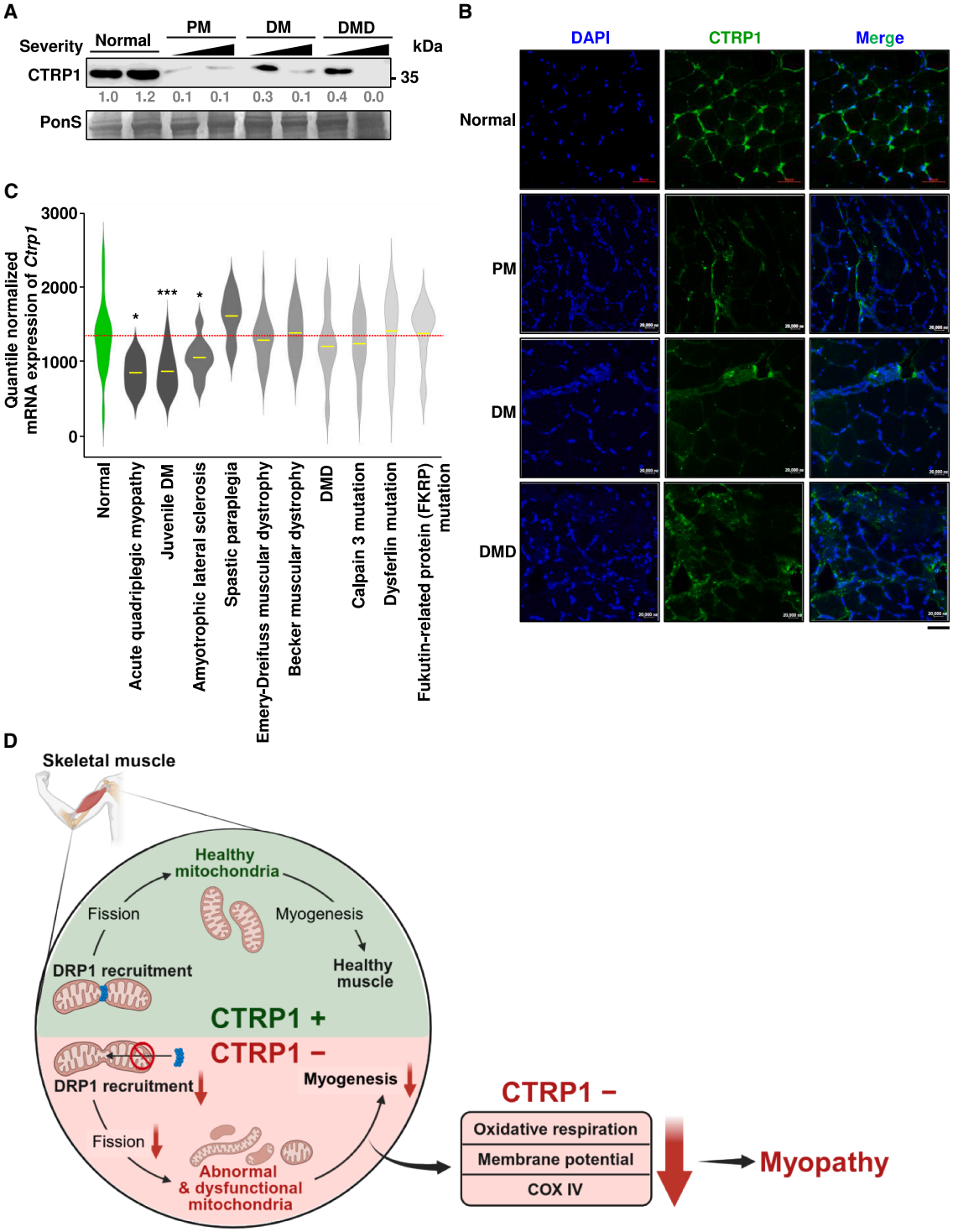


Figure 7. CTRP1 expression is diminished in human myopathy

(A and B) CTRP1 protein levels were analyzed in skeletal muscle tissues from healthy individuals and patients with myopathies using immunoblotting (A) and immunofluorescence (B). Immunoblotting results were normalized and quantified using Ponceau S (PonS) staining as the loading control. CTRP1 protein levels and localization were assessed using immunofluorescence, with DAPI used for DNA counterstaining (scale bar: 40 μm). (C) Comparison of muscular *Ctrp1* mRNA expression across 10 muscle diseases: acute quadriplegic myopathy ($n = 3$), juvenile DM ($n = 20$), amyotrophic lateral sclerosis (ALS; $n = 9$), spastic paraplegia ($n = 4$), Emery-Dreifuss muscular dystrophy

(legend continued on next page)

remained unchanged in skeletal muscle under physiological conditions such as aging, immobilization, and fasting-refeeding (Figures S10A–S10C). In CTRP1 KO$^{\Delta ACTA}$ mice, adipose CTRP1 levels in interscapular BAT (iBAT) and epididymal WAT (eWAT) were unchanged, as expected for a muscle-restriction deletion (Figures S9C–S9E); however, eWAT mass, which normalized to body weight, was modestly reduced (Figures S9F and S9G), and iBAT displayed larger lipid droplets without a mass difference without changes in eWAT and intramuscular adipose tissue (iMAT) (Figure S9H). These findings provide evidence that CTRP1-linked muscle-fat crosstalk can produce depot-specific effects, even without local adipose CTRP1 loss, and that CTRP1-mediated mitochondrial regulation is critical in cellular processes with enormous energy requirements, including muscle regeneration and ATP burning.

Since CTRP1 is enriched in cardiac as well as skeletal muscle[14] and ACTA-Cre can be active in cardiomyocytes, we assessed possible cardiac leakiness in CTRP1 KO$^{\Delta ACTA}$ mice. Cardiac CTRP1 mRNA and protein levels were similar to, or slightly higher than, those of WT mice (Figures S11A–S11C). The small reduction in heart weight disappeared after normalization to body weight (Figure S11D). Histology showed a modest decrease in interventricular septal (IVS) thickness and cardiomyocyte diameter in the left ventricle (LV) and IVS (Figures S11E and S11F). We therefore examined MAPK signaling, a key regulator of hypertrophic growth.[38] In CTRP1 KO$^{\Delta ACTA}$ hearts, p38 phosphorylation was reduced, SAPK/JNK phosphorylation was increased, and ERK1/2 phosphorylation was unchanged (Figure S11G), indicating noncanonical remodeling of MAPK pathways. Given that CTRP1 is a myokine, these changes may reflect skeletal muscle-to-heart paracrine communications. Overall, the skeletal muscle phenotype appears primarily muscle intrinsic, although cardiac contributions cannot be excluded. Echocardiography and pressure-volume analysis, with heart-specific CTRP1 models, will directly assess cardiac involvement in the future.

This study has several limitations. First, our CTX injury model was applied to WT mice; thus, future studies using genetic or inflammatory myopathy models are needed to validate our findings. Second, whereas we demonstrated that CTRP1 regulates DRP1 localization, the precise molecular mechanism, whether through direct interaction, post-translational modification, or the involvement of additional scaffolding proteins, remains unknown. Third, the direct role of CTRP1 at the neuromuscular junction (NMJ) remains unexplored. Given that the synaptic transmission is energetically demanding and NMJ stability depends on mitochondrial dynamics,[39] CTRP1 may influence NMJ integrity through its role in DRP1-dependent fission. Previous neuronal study has shown that ER-associated CTRP1 regulates DRP1 recruitment at ER-mitochondria contact sites,[9] and in this present study, we established a muscle-centered role for CTRP1 in mitochondrial dynamics and myogenic differentiation, with reduced CTRP1 expression in DMD muscles. Although neurons were not examined here, neuron-related GO terms in RNA-seq with CTRP1 KO$^{\Delta ACTA}$ muscle (Figures S5E and S5F) suggest a possible NMJ component and motivate targeted analyses of NMJ structure and function in CTRP1 KO$^{\Delta ACTA}$ mice. Finally, although this study focused on intracellular mechanisms, CTRP1 may also act in an autocrine or paracrine manner during myogenic differentiation because of its secreted nature, potentially affecting the muscle microenvironment.

In conclusion, this study identified CTRP1 as a previously unrecognized regulator of mitochondrial dynamics and skeletal muscle regeneration. By promoting DRP1-dependent fission, preserving mitochondrial quality, and supporting myogenic differentiation, CTRP1 has emerged as a promising therapeutic target for mitochondrial and inflammatory myopathies (Figure 7D). Enhancing CTRP1 expression or activity may provide a multifaceted strategy for restoring mitochondrial function and improving muscle regeneration under pathological conditions.

MATERIALS AND METHODS

Reagents and antibodies

Antimycin A, ascorbate, carbonyl cyanide 4-(trifluoromethoxy) phenylhydrazone (FCCP), dexamethasone, Fluoroshield with DAPI, indomethacine, insulin solution, oligomycin A, Ponceau S solution, rotenone, sodium azide, TMRE, tetramethyl-*p*-phenylenediamine (TMPD), triiodothyronine, and 3-isobutyl-1-methylxanthine were purchased from Sigma-Aldrich (St. Louis, MO, USA) and used at the indicated concentrations. CTX was purchased from MedChemExpress (Cat.# HY-P1902, Monmouth Junction, NJ, USA). Hematoxylin and eosin (H&E) Y solutions were purchased from TissuePro Technology (Gainesville, FL, USA). MitoBrilliant was purchased from Tocris Bioscience (Bristol, UK). Matrigel matrix was purchased from Corning (Corning, NY, USA). MitoTracker Green and MitoTracker Red were purchased from Thermo Fisher Scientific (Waltham, MA, USA). Rat tail collagen was purchased from Corning Life Sciences (Tewksbury, MA, USA). Collagenase type II was purchased from Worthington Biochemical (Vassar Ave, Lakewood, NJ, USA), and Surgipath FSC22 Clear Frozen Section Compound was purchased from Leica Biosystems (Nuβloch, Germany). All the reagents used were of analytical grade. Isoflurane

(n = 22), Becker muscular dystrophy (n = 5), DMD (n = 10), calpain-3 mutation (n = 9), dysferlin mutation (n = 10), Fukutin-related protein (FKRP) mutation (n = 7), and healthy controls (n = 20) from the dataset GEO: GSE3307 (human skeletal muscle). Values are presented as mean ± SD. *$p < 0.05$ and ***$p < 0.001$ compared to healthy controls and indicated myopathy, Dunnett's test. PM, polymyositis; DM, dermatomyositis; DMD, Duchenne muscular dystrophy; PonS, Ponceau S. (D) Proposed role of CTRP1 in the mitochondria-associated myogenic differentiation mechanism. Physiologically, muscular CTRP1 facilitates mitochondrial dynamics by regulating the recruitment of the fission protein DRP1 to the mitochondria, promoting myogenesis. In contrast, muscular CTRP1 deficiency disrupts mitochondrial dynamics, leading to dysfunctional mitochondria and impaired myogenesis, contributing to myopathies. This figure was created using BioRender.com.

Table 1. Mitochondrial involvement in human myopathies

Diseases	Group	Mitochondria involvement
Acute quadriplegic myopathy	acquired myopathy	direct (acquired mitochondrial dysfunction in intensive care unit)[30]
Juvenile dermatomyositis	inflammatory myopathy	direct (mitochondrial dysfunction-upregulated IFN type 1)[31]
Amyotrophic lateral sclerosis	motor neuron disorder	direct (neuronal mitochondrial dysfunction-induced cell death)[32]
Spastic paraplegia	motor neuron disorder	minimal and variable (most are axonal and only sub-types depend on mitochondria, e.g., SPG7)[33]
Emery-Dreifuss muscular dystrophy	muscular dystrophy (structural protein mutation)	possible secondary[34]
Becker muscular dystrophy	muscular dystrophy (structural protein mutation)	possible secondary (ROS and Ca^{2+}-induced mitochondrial dysfunction)[35]
Duchenne muscular dystrophy	muscular dystrophy (structural protein mutation)	possible secondary (ROS and Ca^{2+}-induced mitochondrial dysfunction)[35]
Calpain-3 mutation	limb-girdle muscular dystrophy	possible secondary[36]
Dysferlin mutation	limb-girdle muscular dystrophy	possible secondary[36]
Fukutin-related protein (FKRP) mutation	limb-girdle muscular dystrophy	possible secondary[37]

was purchased from HanaPharm (Gyeonggi-do, Korea). The primary antibodies used for immunoblotting and IF were as follows: α-tubulin (#sc-53646), β-actin (#sc-47778), and myogenin (#sc-12732) (Santa Cruz, Dallas, TX, USA); Cre recombinase (#15036), cytochrome *c* (#4280), COX IV (#4850), UCP1 (#14670), and voltage-dependent anion channel (VDAC; #4661) (Cell Signaling Technology, Danvers, MA, USA); DRP1 (#61113) (BD Biosciences, Becton Drive Franklin Lakes, NJ, USA); myosin heavy chain (slow, α- and β-, type I, #BA-F8), myosin heavy chain type IIA (#SC-71), and myosin heavy chain type IIB (#BF-F3) (Developmental Studies Hybridoma Bank, Iowa City, IA, USA); and goat anti-mouse FITC-conjugated antibody (#A90-116F, Bethyl Laboratories, Montgomery, TX, USA). Secondary antibodies for immunoblotting and IF were purchased as follows: goat anti-mouse HRP-conjugated antibody (#ADI-SAB-100-J) and goat anti-rabbit HRP-conjugated antibody (#ADI-SAB-300-J) (Enzo Life Sciences, Farmingdale, NY, USA); Alexa Fluor 488 goat anti-mouse IgG1 (γ1, #A21121), Alexa Fluor 350 goat anti-mouse IgG2b (γ2b, #A21140), and Alexa Fluor 555 goat anti-mouse IgM (μ chain, #A21426) (Invitrogen, Carlsbad, CA, USA). Mouse anti-human CTRP1 monoclonal antibody (E21H7) and rabbit anti-mouse CTRP1 polyclonal antibody were used as described previously.[40]

ANIMALS

6- to 7-week-old male C57BL/6 WT mice were purchased from DBL (Chungcheongbuk-do, Korea). The mice were acclimatized for 1 week before the experiments commenced. The bedding was changed once a week, and the temperature (22°C–23°C) and humidity (40%–55%) were controlled. Unless otherwise indicated, the mice were housed under 12-h light/12-h dark conditions and were allowed free access to food and water. For tissue harvesting, mice were sacrificed by CO_2 euthanasia, and tissues were immediately frozen in liquid nitrogen and stored at −80°C or fixed in 10% neutral buffered formalin (Sigma-Aldrich). The plans and protocols for the animal experiments were approved by the Institutional Animal Care and Use Committee of Sookmyung Women's University, Seoul, Korea (SMWU-IACUC-1907-018-03).

CTX-induced muscle injury

To induce muscle injury, each mouse was injected with 10 μM CTX into the left gastrocnemius muscle, and tissue samples were collected 3, 5, or 7 days later and analyzed. The right gastrocnemius, which was injected with 10 μM NaCl Veh solution, served as the control.

Immobilization-induced muscle atrophy

The left hindlimbs of C57BL/6 WT mice at 12 weeks old were immobilized using a Manipler AZ device (MANI, Utsunomiya, Tochigi, Japan). Each mouse's foot was folded so that the dorsum of the foot was in contact with the shin, and then it was fastened with a staple. The right hindlimb was used as the control. The immobilization status of the mice was monitored daily, and if a staple was found to be missing from the ankle, immobilization was promptly reapplied. The immobilization was maintained for 2 weeks.

Inverted screen test

Kondziela's inverted screen test was conducted to measure the grip strength of mice using all four limbs by placing the mouse on a square wire screen and rotating it 180°, as described previously.[41] The time until the fall was recorded. The test was performed every other day for 3 days to acclimate the mice to the apparatus.

Grip strength test

The mice were held by the tail and placed on a grid connected to a digital force gauge (Jeung Do Bio & Plant, Seoul, Korea). The maximum grip force was recorded until the limb left the grid by pulling the tail.

Generation of CTRP1 KO$^{\Delta ACTA}$ mice

Floxed mutant mice possessing *LoxP* sites flanking exon 3 of the *Ctrp1* gene (CTRP1$^{f/f}$) were generated as described previously.[14] Skeletal muscle-specific CTRP1-KO mice were generated by breeding CTRP1$^{fl/fl}$ mice with Tg mice expressing Cre recombinase driven by the human alpha-skeletal actin promoter (B6.Cg-Tg (ACTA1-cre) 79Jme/J, ACTA-Cre Tg, The Jackson Lab., Sacramento, CA, USA). The presence of the floxed *Ctrp1* construct and

the ACTA-Cre recombinase construct was confirmed by analyzing the genomic DNA obtained from tail biopsies using the following primer pairs: floxed *Ctrp1* forward, 5′-GGAATGGCTGGCTTA GATTC-3′ and reverse, 5′-GAGGGAGAGAAGAAAGCCTA-3′. The expected product sizes were 1,000 bp for the WT allele and 1,200 bp for the floxed *Ctrp1* allele: ACTA-Cre forward, 5′-GCGGTCTGGCAGTAAAAACTATC-3′ and reverse, 5′-GTAA AACAGCATTGCTGTCACTT-3′. The heterozygous conditional CTRP1-KO mouse line (CTRP1$^{fl/wt}$; ACTA-Cre Tg) was further bred to generate homozygous conditional CTRP1-KO mice (CTRP1$^{fl/fl}$; ACTA-Cre Tg). Age-matched CTRP1$^{fl/fl}$ littermates were used as WT mouse controls, and gender-dependent effects were excluded, as male and female mice were used at a 1:1 ratio. For PCR, an AccuPower 2× PCR master mix (Bioneer, Daejeon, Korea) was used.

Histology

Mouse skeletal muscle tissue was shaped, mounted, and frozen with isopentane, then sectioned into 5-μm-thick sections using a cryostat, as previously described,[42] followed by H&E staining at the Chronic and Metabolic Diseases Research Center (CMDRC) of Sookmyung Women's University (Seoul, Korea). The muscle fiber CSA and fiber numbers were measured using ImageJ software.

TEM

Freshly excised tissues were fixed overnight at 4°C in Karnovsky's fixative. The fixed tissues were washed with 0.05 M sodium cacodylate buffer and post-fixed with 1% osmium tetroxide for 1 h at 4°C. The specimens were then washed with distilled water (DW), and *en bloc* staining was performed in 0.5% uranyl acetate overnight at 4°C. Specimens were washed with DW, dehydrated through an ethanol series, transited with a mixture of propylene oxide and Spurr's resin, and finally polymerized in 100% Spurr's resin overnight at 70°C. The specimens were sectioned using an ultramicrotome (EM UC7; Leica Biosystems). Ultrathin sections were observed using TEM at 120 kV (Talos L120C, Thermo Fisher Scientific). Pre-treatment of tissue, sectioning, and TEM observation were conducted at the National Instrumentation Center for Environmental Management (NICEM) at the College of Agriculture and Life Sciences, Seoul National University (Seoul, Korea). The area and number of IMF mitochondria were measured using ImageJ.

Live micro-CT scanning

In vivo live micro-computed tomography (micro-CT) imaging was performed using a SkyScan1276 system (Bruker microCT, Kontich, Belgium) at the CMDRC, Sookmyung Women's University, to evaluate the CSA of mouse hindlimb muscles. The mice were anesthetized with 2% isoflurane in oxygen and placed in a prone position on the imaging platform. Scanning was conducted at 50 kV and 200 μA using a 0.25 mm aluminum filter with a voxel size of 9 μm. The scan involved a 180° rotation with 0.5° angular increments, and the total acquisition time was approximately 10 min per mouse. The reconstructed images were processed using NRecon and CTAn software (Bruker). Regions of interest (ROIs) were manually defined at the mid-belly of the triceps surae muscle, and CSA was quantified from two-dimensional cross-sectional slices.

Human samples

Two independent skeletal muscle biopsy sets were analyzed. Cohort 1 (expression cohort) comprised samples used to assess CTRP1 protein levels by diagnosis and severity: normal controls (n = 2), PM mild (n = 1), PM severe (n = 1), DM mild (n = 1), DM severe (n = 1), DMD mild (n = 1), and DMD severe (n = 1). Cohort 2 (IF cohort) comprised normal (n = 5), PM (n = 6), DM (n = 5), and DMD (n = 5). All tissue was obtained with informed consent at the Gangnam Severance, College of Medicine, Yonsei University (Seoul, Korea), and the use of patient samples was approved by the Institutional Review Board of Severance Hospital (3-2018-0285). The samples were snap frozen in isopentane and processed for immunoblotting and IF. For IF with patient samples, sliced tissues were fixed with 10% neutral buffered formalin and washed with PBS. Next, the tissues were permeabilized with 0.1% Triton X-100 (Sigma-Aldrich), washed with PBS, blocked in PBS with 0.1% bovine serum albumin (BSA) at 23°C for 30 min, and immunostained with anti-CTRP1 (E21H7) (1:200) at 23°C for 2 h. After incubation, FITC-conjugated secondary antibodies diluted in PBS were applied, and DNA was stained with Fluoroshield with DAPI. Still images were obtained using a confocal laser scanning biological microscope (Olympus FV1000, Tokyo, Japan) at the Core Facility for Supporting Analysis & Imaging of Biomedical Materials, Wonkwang University, supported by the National Research Facilities and Equipment Center (Jeonbuk-do, Korea).

IF

Experiments were performed as previously described.[43] Confocal still images were obtained using a Zeiss confocal microscope (LSM 900, Carl Zeiss Microscopy GmbH, Jena, Germany) at CMDRC, Sookmyung Women's University.

Mouse myofiber-type composition analysis

Immunostaining and analysis of myofiber-type composition were performed as described previously.[44] Briefly, the freshly isolated tissues were snap frozen in isopentane, permeabilized with 0.1% Triton X-100, blocked in PBS with 0.1% BSA at 23°C for 30 min, and immunostained with anti-myosin heavy chain type I (BA-F8, 1:100), type IIA (SC-71, 1:100), and type IIB (BF-F3, 1:100) at 4°C for overnight. After incubation, Alexa Fluor 350 goat anti-mouse IgG2b (γ2b), Alexa Fluor 488 goat anti-mouse IgG1 (γ1), and Alexa Fluor 555 goat anti-mouse IgM (μ) secondary antibodies diluted in PBS were applied to discriminate between each fiber type. The fiber types were analyzed using ImageJ.

Colocalization efficiency of DRP1 and mitochondria

Freshly isolated tissues were fixed in 10% neutral buffered formalin and processed at the CMDRC, Sookmyung Women's University. Formalin-fixed paraffin-embedded (FFPE) specimens were cut into 5-μm-thick sections on HistoBond+R Supercharged tissue slides (Aptum Biologics, Southampton, UK) and deparaffinized, and

antigen retrieval was performed using a TintoRetriever pressure cooker (Bio SB, Santa Barbara, CA, USA) filled with diluted R-Universal Buffer (Aptum Biologics) according to the manufacturer's protocol. Thereafter, 200 nM MitoBrilliant was added and incubated at 37°C for 1 h. After washing with PBS, the specimens were permeabilized with 0.1% Triton X-100, washed with PBS, blocked in PBS with 0.1% BSA at 23°C for 30 min, and immunostained with anti-DRP1 (1:100) antibody at 4°C overnight. After incubation, FITC-conjugated secondary antibodies diluted in PBS were applied, and DNA was stained with Fluoroshield with DAPI. Pearson's colocalization coefficient was analyzed using ImageJ.

In silico analysis

The mRNA expression profiles (dataset GEO: GSE3307)[45,46] were retrieved from the GEO database (http://www.ncbi.nlm.nih.gov/) and analyzed.

Mouse primary cell isolation, culture, and differentiation

Primary myoblasts were isolated from 7-month-old mice and seeded at equal density across groups (1×10^6 cells per well in 6-well plates). Cells were then cultured and differentiated into myotubes as described previously.[47] Primary brown preadipocytes prepared from P2–P3 mice were used. iBAT was harvested, chopped, and incubated at 37°C for 20 min with fresh collagenase type II buffer (123 mM NaCl, 5 mM KCl, 1.3 mM $CaCl_2$, 5 mM D-glucose, 100 mM HEPES [pH 7.4], and 0.2% collagenase type II) for digestion. After incubation, the cell suspension was dissociated with a 70 μm nylon mesh, which was then centrifuged at 200–250*g* for 5 min, washed with high-glucose Dulbecco's modified Eagle's medium (DMEM) supplemented with 20% heat-inactivated fetal bovine serum (FBS; Gibco, Waltham, MA, USA), re-centrifuged, and seeded with high-glucose DMEM supplemented with 20% FBS for passage 0. Cells were cultured to confluence and then exposed to differentiation media (0.5 mM IBMX, 0.125 μM indomethacine, 0.5 μM dexamethasone, 20 nM insulin, 1 nM T3, 1% antibiotics, and high-glucose DMEM supplemented 10% FBS) for 2 days. Cells were then switched to growth media (20 nM insulin, 1 nM T3, 1% antibiotics, and high-glucose DMEM supplemented with 10% FBS) for an additional 4 days, and the growth medium was changed every other day. The expression of UCP1 was analyzed by immunoblotting to ensure successful differentiation into mature brown adipocytes.

Cell culture

The mouse myoblast cell line C2C12, a kind gift from Professor Gyu-Un Bae (College of Pharmacy, Sookmyung Women's University, Seoul, Korea), was cultured in high-glucose DMEM supplemented with 15% heat-inactivated FBS at 37°C in a 5% CO_2 humidified atmosphere. To differentiate C2C12 cells into myotubes, the medium was replaced with high-glucose DMEM supplemented with 2% horse serum. The differentiation medium was changed every other day during the differentiation of myoblasts into myotubes. For plasmid DNA transfection, Lipofectamine 2000 (Thermo Fisher Scientific) was used according to the manufacturer's instructions.

CRISPR-based gene disruption in C2C12 myoblasts

Ctrp1 gene knockdown in C2C12 myoblasts using the CRISPR-Cas9 system was performed according to the methods described previously,[48] with the following modifications: the targeted *Ctrp1* gene knockdown was engineered to span exon 2 and the adjacent intronic region between exons 2 and 3 of the mouse *Ctrp1* gene. The forward and reverse gRNA sequences were designed to flank a 247-nt region within exon 2 (positions 118,334,593 and 118,334,817, respectively, relative to the reference genome NCBI nucleotide accession number: NC_000077.7, chromosome 11). *Ctrp1*-specific gRNAs were designed using the CRISPRscan platform.[49] PCR analysis using forward and reverse probes distinguished the KO cells, showing the expected reduced amplicon size (186 bp, compared to 433 bp in the WT). The design and construction of CRISPR/Cas9-mediated CTRP1 deletion was illustrated in Figure S1. Each 1 μg synthetic sgRNA was incubated with 1 μg Cas9 protein to obtain ribonucleoprotein (RNP) complexes, which were electroporated into C2C12 myoblasts using a Neon transfection kit and device (Invitrogen).

Adenovirus generation

Recombinant adenoviruses expressing mouse *Ctrp1* were generated using the AdEasy adenoviral vector system described previously.[50] Briefly, the mouse *Ctrp1* open reading frame was PCR amplified from the pOptiVec plasmid containing full-length mouse *Ctrp1*[14] using the following primer pairs: forward, 5′-CGGGTCCATGGG CTCCTGTGCA-3′ and reverse, 5′-CGGCGGCCGCCTAGGGCT CAGAGG-3′, and then subcloned into the KpnI-NotI site of pAdTrack shuttle vector. Next, linearized pAdTrack containing full-length mouse *Ctrp1* was transformed into *Escherichia coli* BJ5183AD cells containing the adenoviral backbone plasmid pAdEasy-1 for homologous recombination. A positive 3 μg recombinant plasmid was linearized with PacI and transfected into HEK293A packaging cells (American Type Culture Collection, Manassas, VA, USA). Recombinant adenoviruses expressing mouse *Ctrp1* were purified by CsCl banding, mixed with storage buffer (10 mM Tris [pH 8.0], 100 mM NaCl, 0.1% BSA, and 50% glycerol), and stored at −80°C until use.

Extracellular flux analysis

The OCR and COX IV activity were measured using an XFe24 analyzer (Seahorse Bioscience, North Billerica, MA, USA) according to the manufacturer's protocol at the CMDRC, Sookmyung Women's University, as previously described,[47] with the following modifications. Mouse primary myoblasts were incubated in Matrigel-coated wells at 37°C in a humidified 5% CO_2 incubator. To measure the OCR, 2 μM oligomycin A, 5 μM FCCP, and 0.5 μM rotenone/antimycin A were injected in that order into each well. To measure COX IV activity, 0.5 μM rotenone/antimycin A, 150 μM TMPD/10 μM sodium azide, and 5 mM sodium azide were injected into each well in that order. XF DMEM medium (Seahorse Bioscience) supplemented with 10 mM glucose, 2.5 mM glutamine, and 1 mM sodium pyruvate was used for both OCR and COX IV activity assays. The raw data were normalized to the protein concentration of whole-cell lysates.

Mitochondria staining (TMRE, MitoTracker Green, MitoTracker Red CMXRos, and MitoBrilliant)

Mitochondrial staining in living cells was performed using TMRE, MitoTracker Green, and MitoTracker Red CMXRos reagents according to the manufacturer's protocol to analyze mitochondrial potential (TMRE and MitoTracker Red) and mass (MitoTracker Green). MitoBrilliant was used to measure the mitochondrial mass in fixed tissue according to the manufacturer's protocol. TMRE fluorescence was immediately measured at Ex/Em = 549/575 nm using a microplate reader after the normalization of the protein concentration. MitoTracker Red CMXRos fluorescence in live C2C12 cells was immediately measured using FACS Calibur (BD Bioscience) at the Gyeongnam Bio and Anti-aging Core Facility Center, Changwon National University (Gyeongsangnam-do, Korea). Cell images were acquired using a Zeiss LSM 700 confocal microscope (Carl Zeiss Microscopy) at the CMDRC, Sookmyung Women's University, and analyzed using ZEN software as previously described.[47]

Mitochondria isolation and transfer

Mouse primary myoblasts were harvested with ice-cold mitochondria isolation buffer (MIB; 0.025 M Tris [pH 7.4], 0.25 M sucrose, and 1 mM EDTA), passed through a 23G needle using a syringe 10 times on ice, and centrifuged at 3,000 rpm for 10 min at 4°C. The supernatant was centrifuged at 9,500 rpm for 10 min at 4°C. The pellet from centrifugation was re-homogenized in ice-cold MIB three times, followed by centrifugation at 2,500 rpm for 10 min at 4°C. The supernatant was discarded, and the mitochondria-containing pellet was resuspended in ice-cold MIB and subsequently centrifuged at 6,500 rpm for 10 min at 4°C. The mitochondrial pellet was washed three times with ice-cold MIB, consisting of three repetitions of resuspension with a Pasteur pipette and centrifugation at 6,500 rpm for 10 min at 4°C each. The washed mitochondrial pellet was then resuspended in ice-cold culture media for mouse primary myoblasts (DMEM/F12 supplemented with 30% FBS and AminoMAX), homogenized at low speed to achieve a well-suspended solution, and quantified and normalized for immediate transfer to recipient primary myoblasts, as described previously.[51] Mitochondrial transfer was performed using unlabeled mitochondria and cells for the biological characterization of the recipient cells, as previously described.[51]

RT-qPCR

RNA isolation, RT, and PCR measurements were using 2× Fast Q-PCR Master Mix (SMOBIO Technology, Hsinchu, Taiwan) and an Applied Biosystems QuantStudio 3 Real-Time PCR System (Thermo Fisher Scientific). The *Ct* values were normalized to β-actin mRNA levels (Δ*Ct*), and relative mRNA expression levels were calculated using the formula $2^{-\Delta\Delta Ct}$ ($2^{-(Ct\ \text{experimental} - Ct\ \text{control})}$). Appropriate primer pairs for mouse mRNA samples were used as follows: *β-actin* forward, 5′-TGTCCACCTTCCAGCAGATGT-3′ and reverse, 5′-AGCTCAGTAACAGTCCGCCTAGA-3′; *Ctrp1* forward, 5′-CAATTCCTCCACCCCAGAT-3′ and reverse, 5′-CCCCTCGGTCACCTTTCT-3′; *Pax7* forward, 5′-AGGCAGCAAGCCCAGACAGGTG-3′ and reverse, 5′-TAATCG AACTCACTGAGGGCACCGT-3′; *MyoD* forward, 5′- AAACCCCAATGCGATTTATCAGG-3′ and reverse, 5′-TAAGCTTCATCTTTTGGGCGTGA-3′; *Myogenin* forward, 5′-ACAGCATCACGGTGGAGGATATGT-3′ and reverse, 5′-CCCTGCTACAGAAGTGATGGCTTT-3′; *Myh2* forward, 5′-AAGTGACTGTGAAAACAGAAGCA-3′ and reverse, 5′-GCAGCCATTTGTAAGGGTTGAC-3′; *Myh4* forward, 5′-CAGGACTTGGTGGACAAACTACA-3′ and reverse, 5′-TTTAGTGTGAACCTCTCGGCTC-3′; *MAFbx* forward, 5′-GAAGAGAGCAGTATGGGGTCAC-3′ and reverse, 5′-CTTGAGGGGAAAGTGAGACG-3′; and *Murf1* forward, 5′-TGACATCTACAAGCAGGAGTGC-3′ and reverse, 5′-TCGTCTTCGTGTTCCTTGC-3′.

Quantification of mtDNA

Total genomic DNA was extracted from the triceps surae using the AccuPrep Genomic DNA Extraction Kit (Bioneer) according to the manufacturer's protocol. The expression levels of *NADH dehydrogenase subunit 1* (mtDNA) were quantified by qPCR and normalized with *Lpl* (genomic DNA) using primer pairs as previously described[52] as follows: mtDNA forward, 5′-CCCATTCGC GTTATTCTT-3′ and reverse, 5′-AAGTTGATCGTAACGGAAGC-3′, and *Lpl* forward, 5′-GGATGGACGGTAAGAGTGATTC-3′ and reverse, 5′-ATCCAAGGGTAGCAGACAGGT-3′.

Protein extraction and immunoblotting

Protein extracts were obtained from cultured cells or animal tissues in GST-IP buffer (50 mM Tris-HCl [pH 7.5], 150 mM NaCl, 1 mM EDTA, 0.5% NP-40, and Complete Protease Inhibitor Cocktail Tablets [Roche, Basel, Switzerland]) or RIPA buffer (20 mM Tris-HCl [pH 7.5], 150 mM NaCl, 1 mM EDTA, 1% NP-40, 1% sodium dodecyl sulfate [SDS], and Complete Protease Inhibitor Cocktail Tablets [Roche]), respectively. Protein extracts were then mixed with 5× SDS sample buffer. Immunoblotting was performed, and peroxidase activity was quantified using ImageJ software. Peroxidase activity was visualized using an ECL kit (Bionote, Gyeonggi-do, Korea), and PonS, α-tubulin, or β-actin levels were analyzed as loading controls. The results shown represent two to three independent experiments.

Statistics

Values are presented as mean ± standard deviation (SD). All biochemical analyses were performed at least in duplicate. Multiple comparisons within groups were performed using one-way analysis of variance (ANOVA), and individual group mean differences were evaluated using the two-tailed Student's *t* test and Tukey's test. A maximum level of significance of $p < 0.05$ was used for all statistical comparisons. Pearson's correlation coefficients were calculated to evaluate the association between DRP1 and mitochondrial localization. All statistical analyses were performed using GraphPad Prism v. 10 for Windows (GraphPad Software).

Data and code availability

The data supporting the findings of this study are available from the corresponding author upon reasonable request.

ACKNOWLEDGMENTS

This research was supported by the National Research Foundation of Korea, funded by the Ministry of Education (RS-2023-00246963, 2021R1A2C3003414, and 2021R1A6A1A03038890), and by a Korea Basic Science Institute (National Research Facilities and Equipment Center) grant funded by the Ministry of Education (RS-2021-NF000716 and RS-2024-00436674).

AUTHOR CONTRIBUTIONS

S.H. designed and performed the experiments and wrote the manuscript. Y.Y. designed and supervised the research and wrote the manuscript. Y. Jang, H.J.J., H.-A.N., Y. Jung, and D.P. performed the experiments. H.I.K., S.H.M., D.K., B.R.S., and S.-E.K. contributed materials and analyzed the data. S.K.S., G.T.O., and S.-Y.P. contributed to the generation of the mouse model. Y.-C.C. contributed to clinical assessments.

DECLARATION OF INTERESTS

The authors declare no conflicts of interest.

SUPPLEMENTAL INFORMATION

Supplemental information can be found online at https://doi.org/10.1016/j.ymthe.2025.12.063.

REFERENCES

1. Nagy, H., and Veerapaneni, K.D. (2024). Myopathy (StatPearls Publishing).
2. Arena, I.G., Pugliese, A., Volta, S., Toscano, A., and Musumeci, O. (2022). Molecular genetics overview of primary mitochondrial myopathies. J. Clin. Med. *11*, 632. https://doi.org/10.3390/jcm11030632.
3. Sorrentino, V., Menzies, K.J., and Auwerx, J. (2018). Repairing mitochondrial dysfunction in disease. Annu. Rev. Pharmacol. Toxicol. *58*, 353–389.
4. Lin, F., Sun, L., Zhang, Y., Gao, W., Chen, Z., Liu, Y., Tian, K., Han, X., Liu, R., Li, Y., and Shen, L. (2024). Mitochondrial stress response and myogenic differentiation. Front. Cell Dev. Biol. *12*, 1381417.
5. Kraus, F., Roy, K., Pucadyil, T.J., and Ryan, M.T. (2021). Function and regulation of the divisome for mitochondrial fission. Nature *590*, 57–66.
6. Favaro, G., Romanello, V., Varanita, T., Andrea Desbats, M., Morbidoni, V., Tezze, C., Albiero, M., Canato, M., Gherardi, G., De Stefani, D., et al. (2019). DRP1-mediated mitochondrial shape controls calcium homeostasis and muscle mass. Nat. Commun. *10*, 2576–2579.
7. Otera, H., Miyata, N., Kuge, O., and Mihara, K. (2016). Drp1-dependent mitochondrial fission via MiD49/51 is essential for apoptotic cristae remodeling. J. Cell Biol. *212*, 531–544.
8. Loson, O.C., Song, Z., Chen, H., and Chan, D.C. (2013). Fis1, mff, MiD49, and MiD51 mediate Drp1 recruitment in mitochondrial fission. Mol.Biol.Cell *24*, 659–667.
9. Sonn, S.K., Seo, S., Yang, J., Oh, K.S., Chen, H., Chan, D.C., Rhee, K., Lee, K.S., Yang, Y., and Oh, G.T. (2021). ER-associated CTRP1 regulates mitochondrial fission via interaction with DRP1. Exp. Mol. Med. *53*, 1769–1780.
10. Peterson, J.M., Aja, S., Wei, Z., and Wong, G.W. (2012). CTRP1 protein enhances fatty acid oxidation via AMP-activated protein kinase (AMPK) activation and acetyl-CoA carboxylase (ACC) inhibition. J. Biol. Chem. *287*, 1576–1587.
11. Xin, Y., Zhang, D., Fu, Y., Wang, C., Li, Q., Tian, C., Zhang, S., and Lyu, X. (2017). C1qTNF-related protein 1 improve insulin resistance by reducing phosphorylation of serine 1101 in insulin receptor substrate 1. Endocr. J. *64*, 787–796.
12. Xin, Y., Lyu, X., Wang, C., Fu, Y., Zhang, S., Tian, C., Li, Q., and Zhang, D. (2014). Elevated circulating levels of CTRP1, a novel adipokine, in diabetic patients. Endocr. J. *61*, 841–847.
13. Han, S., Kim, J.D., Lee, S., Jeong, A.L., Park, J.S., Yong, H.J., Boldbaatar, A., Ka, H.I., Rhee, E.J., Lee, W.Y., and Yang, Y. (2016). Circulating CTRP1 levels in type 2 diabetes and their association with FGF21. Int. J. Endocrinol. *2016*, 5479627.
14. Han, S., Jeong, A.L., Lee, S., Park, J.S., Buyanravjikh, S., Kang, W., Choi, S., Park, C., Han, J., Son, W.C., et al. (2018). C1q/TNF-alpha-related protein 1 (CTRP1) maintains blood pressure under dehydration conditions. Circ. Res. *123*, e5–e19.
15. Charge, S.B.P., and Rudnicki, M.A. (2004). Cellular and molecular regulation of muscle regeneration. Physiol.Rev. *84*, 209–238.
16. Schiaffino, S., and Reggiani, C. (2011). Fiber types in mammalian skeletal muscles. Physiol. Rev. *91*, 1447–1531.
17. Yasuda, T., Ishihara, T., Ichimura, A., and Ishihara, N. (2023). Mitochondrial dynamics define muscle fiber type by modulating cellular metabolic pathways. Cell Rep. *42*, 112434.
18. Kim, J.Y., Kang, Y.C., Kim, M.J., Kim, S.U., Kang, H.R., Yeo, J.S., Kim, Y., Yu, S.H., Song, B., Hwang, J.W., et al. (2025). Mitochondrial transplantation as a novel therapeutic approach in idiopathic inflammatory myopathy. Ann. Rheum. Dis. *84*, 609–619.
19. Han, S., and Yang, Y. (2018). A novel blood pressure modulator C1q/TNF-alpha-related protein 1 (CTRP1). BMB Rep. *51*, 611–612.
20. Leveille, C.F., Mikhaeil, J.S., Turner, K.D., Silvera, S., Wilkinson, J., and Fajardo, V.A. (2017). Mitochondrial cristae density: A dynamic entity that is critical for energy production and metabolic power in skeletal muscle. J. Physiol. *595*, 2779–2780.
21. Hong, X., Isern, J., Campanario, S., Perdiguero, E., Ramírez-Pardo, I., Segalés, J., Hernansanz-Agustín, P., Curtabbi, A., Deryagin, O., Pollán, A., et al. (2022). Mitochondrial dynamics maintain muscle stem cell regenerative competence throughout adult life by regulating metabolism and mitophagy. Cell Stem Cell *29*, 1506–1508.
22. Ge, P., Dawson, V.L., and Dawson, T.M. (2020). PINK1 and parkin mitochondrial quality control: A source of regional vulnerability in parkinson's disease. Mol. Neurodegener. *15*, 20–27.
23. Hyatt, H.W., and Powers, S.K. (2021). Mitochondrial dysfunction is a common denominator linking skeletal muscle wasting due to disease, aging, and prolonged inactivity. Antioxidants (Basel) *10*, 588. https://doi.org/10.3390/antiox10040588.
24. Zammit, P.S., Relaix, F., Nagata, Y., Ruiz, A.P., Collins, C.A., Partridge, T.A., and Beauchamp, J.R. (2006). Pax7 and myogenic progression in skeletal muscle satellite cells. J. Cell Sci. *119*, 1824–1832.
25. Katsetos, C.D., Koutzaki, S., and Melvin, J.J. (2013). Mitochondrial dysfunction in neuromuscular disorders. Semin. Pediatr. Neurol. *20*, 202–215.
26. Zhang, H., Zhang-Sun, Z.Y., Xue, C.X., Li, X.Y., Ren, J., Jiang, Y.T., Liu, T., Yao, H.R., Zhang, J., Gou, T.T., et al. (2023). CTRP family in diseases associated with inflammation and metabolism: Molecular mechanisms and clinical implication. Acta Pharmacol. Sin. *44*, 710–725.
27. Deprez, A., Orfi, Z., Rieger, L., and Dumont, N.A. (2023). Impaired muscle stem cell function and abnormal myogenesis in acquired myopathies. Biosci. Rep. *43*, BSR20220284. https://doi.org/10.1042/BSR20220284.
28. Wang, S., Tang, Y., Chen, X., Song, S., Chen, X., Zhou, Q., and Zeng, L. (2024). Mitochondrial-related hub genes in dermatomyositis: Muscle and skin datasets-based identification and in vivo validation. Front. Genet. *15*, 1325035.
29. Bez Batti Angulski, A., Hosny, N., Cohen, H., Martin, A.A., Hahn, D., Bauer, J., and Metzger, J.M. (2023). Duchenne muscular dystrophy: Disease mechanism and therapeutic strategies. Front. Physiol. *14*, 1183101.
30. Klawitter, F., Ehler, J., Bajorat, R., and Patejdl, R. (2023). Mitochondrial dysfunction in intensive care unit-acquired weakness and critical illness myopathy: A narrative review. Int. J. Mol. Sci. *24*, 5516. https://doi.org/10.3390/ijms24065516.
31. Wilkinson, M.G.L., Moulding, D., McDonnell, T.C.R., Orford, M., Wincup, C., Ting, J.Y.J., Otto, G.W., Restuadi, R., Kelberman, D., Papadopoulou, C., et al. (2023). Role of CD14+ monocyte-derived oxidised mitochondrial DNA in the inflammatory interferon type 1 signature in juvenile dermatomyositis. Ann. Rheum. Dis. *82*, 658–669.
32. Cunha-Oliveira, T., Montezinho, L., Simões, R.F., Carvalho, M., Ferreiro, E., and Silva, F.S.G. (2024). Mitochondria: A promising convergent target for the treatment of amyotrophic lateral sclerosis. Cells *13*, 248. https://doi.org/10.3390/cells13030248.
33. Blackstone, C. (2012). Cellular pathways of hereditary spastic paraplegia. Annu. Rev. Neurosci. *35*, 25–47.
34. Helbling-Leclerc, A., Bonne, G., and Schwartz, K. (2002). Emery-dreifuss muscular dystrophy. Eur. J. Hum. Genet. *10*, 157–161.
35. Wilson, K., Faelan, C., Patterson-Kane, J.C., Rudmann, D.G., Moore, S.A., Frank, D., Charleston, J., Tinsley, J., Young, G.D., and Milici, A.J. (2017). Duchenne and becker

muscular dystrophies: A review of animal models, clinical end points, and biomarker quantification. Toxicol. Pathol. *45*, 961–976.

36. Laval, S.H., and Bushby, K.M.D. (2004). Limb-girdle muscular dystrophies–from genetics to molecular pathology. Neuropathol. Appl. Neurobiol. *30*, 91–105.

37. Ortiz-Cordero, C., Azzag, K., and Perlingeiro, R.C.R. (2021). Fukutin-related protein: From pathology to treatments. Trends Cell Biol. *31*, 197–210.

38. Xu, Q., Ding, H., Li, S., Dong, S., Li, L., Shi, B., Zhong, M., and Zhang, G. (2021). Sleeve gastrectomy ameliorates diabetes-induced cardiac hypertrophy correlates with the MAPK signaling pathway. Front. Physiol. *12*, 785799.

39. Miao, Y., Xie, L., Song, J., Cai, X., Yang, J., Ma, X., Chen, S., and Xie, P. (2024). Unraveling the causes of sarcopenia: Roles of neuromuscular junction impairment and mitochondrial dysfunction. Physiol. Rep. *12*, e15917.

40. Kim, K.y., Kim, H.Y., Kim, J.H., Lee, C.H., Kim, D.H., Lee, Y.H., Han, S.H., Lim, J.S., Cho, D.H., Lee, M.S., et al. (2006). Tumor necrosis factor-alpha and interleukin-1beta increases CTRP1 expression in adipose tissue. FEBS Lett. *580*, 3953–3960.

41. Deacon, R.M.J. (2013). Measuring the strength of mice. J. Vis. Exp. *76*, 2610. https://doi.org/10.3791/2610.

42. Terry, R.L., and Wells, D.J. (2016). Histopathological evaluation of skeletal muscle with specific reference to mouse models of muscular dystrophy. Curr. Protoc. Mouse Biol. *6*, 343–363.

43. Jeong, A.L., Lee, S., Park, J.S., Han, S., Jang, C.Y., Lim, J.S., Lee, M.S., and Yang, Y. (2014). Cancerous inhibitor of protein phosphatase 2A (CIP2A) protein is involved in centrosome separation through the regulation of NIMA (never in mitosis gene A)-related kinase 2 (NEK2) protein activity. J. Biol. Chem. *289*, 28–40.

44. Tyagi, S., Beqollari, D., Lee, C.S., Walker, L.A., and Bannister, R.A. (2017). Semi-automated analysis of mouse skeletal muscle morphology and fiber-type composition. J. Vis. Exp. *126*, 56024. https://doi.org/10.3791/56024.

45. Dadgar, S., Wang, Z., Johnston, H., Kesari, A., Nagaraju, K., Chen, Y.W., Hill, D.A., Partridge, T.A., Giri, M., Freishtat, R.J., et al. (2014). Asynchronous remodeling is a driver of failed regeneration in duchenne muscular dystrophy. J. Cell Biol. *207*, 139–158.

46. Bakay, M., Wang, Z., Melcon, G., Schiltz, L., Xuan, J., Zhao, P., Sartorelli, V., Seo, J., Pegoraro, E., Angelini, C., et al. (2006). Nuclear envelope dystrophies show a transcriptional fingerprint suggesting disruption of rb-MyoD pathways in muscle regeneration. Brain *129*, 996–1013.

47. Joo, H.J., D'Alessandro, M., Oh, G., Han, S., Kim, W.J., Chung, G.E., Jang, Y., Lee, J. B., Lee, C., and Yang, Y. (2024). Novel targets of beta-TrCP cooperatively accelerate carbohydrate and fatty acid consumption. J. Cell. Physiol. *239*, e31095.

48. Gundry, M.C., Brunetti, L., Lin, A., Mayle, A.E., Kitano, A., Wagner, D., Hsu, J.I., Hoegenauer, K.A., Rooney, C.M., Goodell, M.A., and Nakada, D. (2016). Highly efficient genome editing of murine and human hematopoietic progenitor cells by CRISPR/Cas9. Cell Rep. *17*, 1453–1461.

49. Moreno-Mateos, M.A., Vejnar, C.E., Beaudoin, J.D., Fernandez, J.P., Mis, E.K., Khokha, M.K., and Giraldez, A.J. (2015). CRISPRscan: Designing highly efficient sgRNAs for CRISPR-Cas9 targeting in vivo. Nat. Methods *12*, 982–988.

50. Luo, J., Deng, Z.L., Luo, X., Tang, N., Song, W.X., Chen, J., Sharff, K.A., Luu, H.H., Haydon, R.C., Kinzler, K.W., et al. (2007). A protocol for rapid generation of recombinant adenoviruses using the AdEasy system. Nat. Protoc. *2*, 1236–1247.

51. Caicedo, A., Fritz, V., Brondello, J.M., Ayala, M., Dennemont, I., Abdellaoui, N., de Fraipont, F., Moisan, A., Prouteau, C.A., Boukhaddaoui, H., et al. (2015). MitoCeption as a new tool to assess the effects of mesenchymal stem/stromal cell mitochondria on cancer cell metabolism and function. Sci. Rep. *5*, 9073.

52. Maurya, S.K., Herrera, J.L., Sahoo, S.K., Reis, F.C.G., Vega, R.B., Kelly, D.P., and Periasamy, M. (2018). Sarcolipin signaling promotes mitochondrial biogenesis and oxidative metabolism in skeletal muscle. Cell Rep. *24*, 2919–2931.